

Flexible space-time models for extreme data

Lorenzo Dell’Oro^a, Carlo Gaetan^b

^a*Dipartimento di Scienze Statistiche, Università di Padova, Padova, Italy*

^b*Dipartimento di Scienze Ambientali, Informatica e Statistica, Università Ca’ Foscari di Venezia, Venezia, Italy*

Abstract

Extreme value analysis is an essential methodology in the study of rare and extreme events, which hold significant interest in various fields, particularly in the context of environmental sciences. Models that employ the exceedances of values above suitably selected high thresholds possess the advantage of capturing the “sub-asymptotic” dependence of data. This paper presents an extension of spatial random scale mixture models to the spatio-temporal domain. A comprehensive framework for characterizing the dependence structure of extreme events across both dimensions is provided. Indeed, the model is capable of distinguishing between asymptotic dependence and independence, both in space and time, through the use of parametric inference. The high complexity of the likelihood function for the proposed model necessitates a simulation approach based on neural networks for parameter estimation, which leverages summaries of the sub-asymptotic dependence present in the data. The effectiveness of the model in assessing the limiting dependence structure of spatio-temporal processes is demonstrated through both simulation studies and an application to rainfall datasets.

Keywords: Asymptotic dependence and independence, Neural networks, Rainfall data, Simulation-based inference, Spatio-temporal extremes, Threshold exceedances

1. Introduction

The analysis of spatial extreme data has received a significant boost because many natural extreme hazards, such as heat waves, heavy rain and snowfall, high tides, and windstorms, have a spatial extent. A significant portion of the research has focused on the development of spatial models grounded in the theory of extreme values, including max-stable processes (de Haan, 1984; Smith, 1990; Schlather, 2002). These processes emerge as the pointwise maxima taken over an infinite number of independent copies of appropriately rescaled stochastic processes. In addition to the solid theoretical arguments, the widespread use of these models is also due to the possibility of estimating their parameters in a relatively simple way, at least for a not large number of sites (Padoan et al., 2010; Castruccio et al., 2016).

Other spatial statistical models for extreme data (Davison et al., 2012; Huser and Wadsworth, 2020) have roots in hierarchical models (Casson and Coles, 1999; Cooley et al., 2007; Gaetan and Grigoletto, 2007; Sang and Gelfand, 2009) and copula models (Bortot et al., 2000; Sang and Gelfand, 2010).

In a recent paper [Huser et al. \(2025\)](#) argue that although the max-stable processes as models are supported by a well-established asymptotic theory, in environmental studies exhibit some restrictions. Since max-stable processes are defined in terms of block maxima at each location, they are not intended to describe the stochastic variability of the extremes of the original individual events. Moreover, max-stable processes attempt to characterize the extremal dependence of the normalized maxima as the block size grows to infinity. In such a situation, two cases arise: dependence in the limit, i.e., asymptotic dependence, or exact independence, i.e., for any block size. However, what is often observed in reality is a third situation, in which the dependence vanishes in the limit (asymptotic independence), but is still present for finite block size (sub-asymptotic dependence). For this reason, several attempts are made to build sub-asymptotic models for spatial extremes based on the exceedances of high thresholds, combining tail flexibility with computational tractability, see for example [Wadsworth and Tawn \(2012\)](#); [Bacro et al. \(2016\)](#); [Huser et al. \(2017\)](#); [Huser and Wadsworth \(2019\)](#); [Wadsworth and Tawn \(2022\)](#).

If the interest is to model the extremes of the original events, a further complication arises when dealing with spatio-temporal data. Many spatial models are fitted by ignoring the temporal dependence of the extremes and then adjusting the uncertainty of the parameter estimates ([Fawcett and Walshaw, 2006](#)). Modeling the spatio-temporal extremal dependence adds an extra layer of difficulties ([Steinkohl et al., 2013](#); [Huser and Davison, 2014](#); [Morris et al., 2017](#); [Tawn et al., 2018](#); [Bacro et al., 2020](#)). In fact, different forms of asymptotic dependence could arise in the spatial and temporal domains. The limiting class could itself change with the temporal and/or spatial lag. In the aforementioned references, the models maintain the same limiting dependence in both space and time.

Recently, [Simpson and Wadsworth \(2021\)](#), [Simpson et al. \(2023\)](#) provide examples of formulations for threshold exceedances that allow for different forms of extremal dependence in the two domains. These papers use a conditional approach based on an asymptotic approximation of the distribution of the space-time process conditional on a single location and time. The construction is highly flexible; however, it is unclear whether a unique space-time process exists, given that the specification is conditional.

Similarly, [Bortot and Gaetan \(2024\)](#) employ a time series approach, wherein extreme spatial dependence is integrated into a time series model ([Davis and Mikosch, 2008](#)). One of the advantages of the proposed model is that it allows for straightforward simulation, thereby facilitating the extrapolation of extremal functionals of interest. Nevertheless, this approach is limited in that the specific type of extremal dependence in the two domains must be predetermined, and the space-time interactions lack sufficient flexibility.

[Huser and Wadsworth \(2019\)](#) introduced a scale mixture model that considers many different possibilities within the spatial framework. These possibilities range from the limit of asymptotic independence to the limit of complete dependence. Subsequently, the spatial model was modified by [Zhang et al. \(2022\)](#) for higher-dimensional inference, and extended by [Majumder et al. \(2024\)](#) to enable enhanced flexibility in the spatial dependence, and by [Majumder and Reich \(2023\)](#) to accommodate dynamic spatial dependencies over time.

In this paper, we propose ways to extend the scale mixture model to include spatial

and temporal dimensions, which would allow greater flexibility than the space-time models previously considered in [Bortot and Gaetan \(2024\)](#), since the models presented here include both extremal dependence classes according to the value of a parameter that can be identified from the data.

The proposed models are employed as copula models and they are subsequently applied to a real data set. However, likelihood-based inference for the parameters of the models becomes infeasible even for moderate sample sizes.

As the simulation of data from the proposed models is a relatively straightforward and rapid process, the parameter estimation is founded on a simulation-based methodology which employs neural networks to learn the implicit mapping between the simulated data and the parameter values ([Gerber and Nychka, 2021](#); [Lenzi et al., 2023](#); [Richards et al., 2024](#); [Sainsbury-Dale et al., 2024](#)). Other recent works that make use of neural networks to identify the extremal dependence of spatial data include [Ahmed et al. \(2022\)](#) and [Wixson and Cooley \(2024\)](#).

The remainder of the paper is organized as follows: in [Section 2](#), we introduce our model. [Section 3](#) presents and discusses parameter estimation using neural networks. The estimation procedure is evaluated in [Section 4](#) through a small simulation study and an analysis of precipitation data from a dataset of rainfall amounts recorded at weather stations in the North Brabant province of the Netherlands. The paper concludes in [Section 5](#).

2. A model for space-time extreme values

We will consider $Y(s, t)$ $s \in S$ as a spatio-temporal process on the geographic space $S \subset \mathbb{R}^d$ and observed at times $t \in \mathcal{T}$, with $\mathcal{T} = \{1, 2, \dots\}$. To model the spatio-temporal extremal dependence of $Y(s, t)$, we follow a copula-based approach: first, we define a process, $X(s, t)$, with a suitable extremal dependence structure, and then we marginally transform it into $Y(s, t)$. Moreover, since the goal is to model only extreme values, we set a high threshold and consider the values that exceed this threshold, while censoring the other observations. In this section, we focus on the specification of $X(s, t)$, leaving the details of marginal transformation to the data application ([Section 4](#)).

We begin by recalling some background material on extremal dependence.

2.1. Asymptotic dependence and independence classes

Let $X_1 := X(s_1, t_1)$ and $X_2 := X(s_2, t_2)$ be a generic pair of random variables of a space-time process $X(s, t)$ with marginal distribution functions F_{X_1} and F_{X_2} , respectively. The strength of dependence in the upper tail of (X_1, X_2) is commonly quantified in terms of the tail dependence coefficient, $\chi \in [0, 1]$, defined as the limit of

$$\chi(u) = \frac{\mathbb{P}(F_{X_1}(X_1) > u, F_{X_2}(X_2) > u)}{1 - u}$$

when this limit exists ([Joe, 1997](#)), i.e.

$$\chi = \lim_{u \rightarrow 1^-} \chi(u) = \lim_{x \rightarrow \infty} \frac{\mathbb{P}(X_1 > x, X_2 > x)}{\mathbb{P}(X_1 > x)}. \quad (1)$$

The last equivalence holds if we assume the marginal distribution of $X(s, t)$ to be stationary over \mathcal{S} and \mathcal{T} , with the upper endpoint at infinity.

When $\chi > 0$, the components of (X_1, X_2) are said to be asymptotically dependent (AD) in the upper tail, and when $\chi = 0$, they are said to be asymptotically independent (AI).

In the latter case it is useful to consider the rate at which the subasymptotic measure $\chi(u)$ tends to zero as $u \rightarrow 1^-$. Following [Ledford and Tawn \(1996\)](#) we may assume that

$$\chi(u) \sim \ell((1-u)^{-1}) (1-u)^{1/\eta-1}, \quad (2)$$

where $\ell(\cdot)$ is a slowly varying function at infinity, that is, $\ell(tx)/\ell(x) \rightarrow 1$ as $x \rightarrow \infty$ for all $t > 0$. The coefficient $0 < \eta \leq 1$ is called the residual tail dependence coefficient. When $\eta = 1$ and $\lim_{u \rightarrow 1^-} \ell((1-u)^{-1}) \neq 0$ we obtain AD, but otherwise there is AI. The case $\eta < 1$ may be further classified into (a) positive association with $0.5 < \eta < 1$; (b) near-independence with $\eta = 0.5$; and (c) negative association with $0 < \eta < 0.5$. Here, for notation simplicity, we have omitted any reference to the pair (X_1, X_2) when defining $\chi(u)$, χ , η and ℓ .

Finally, we say that the process $X(s, t)$ is asymptotically independent (AI) or asymptotically dependent (AD) if η is either strictly less than 1 or equal to 1, respectively, for all pairs (X_1, X_2) . Moreover we say that the process $X(s, t)$ is AI or AD in space if η is either strictly less than 1 or equal to 1, respectively, for all pairs $(X(t, s_1), X(t, s_2))$. Similar definition can be stated in case of the time.

2.2. Model definition

Our starting point is the spatial scale mixture model proposed by [Huser and Wadsworth \(2019\)](#), namely

$$X(s) = R^\delta W(s)^{1-\delta}, \quad \delta \in [0, 1], \quad (3)$$

where R is a standard Pareto random variable, i.e. $\mathbb{P}(R \leq r) = 1 - r^{-1}$, $r \geq 1$, and $W(s)$ is an AI spatial process, independent of R , whose marginal distribution is also standard Pareto. The strength of this specification is that it can cover the AD and AI case according the value of δ . More precisely, [Huser and Wadsworth \(2019\)](#) show that if $\delta > 0.5$ then $X(s)$ is AD, while if $\delta \leq 0.5$, $X(s)$ is AI.

A direct extension of the model (3) for space-time data would be $X(s, t) = R^\delta W(s, t)^{1-\delta}$, $\delta \in [0, 1]$, where $W(s, t)$ is a space-time process. This model would be characterized by either asymptotic dependence in both space and time, or asymptotic independence in both space and time, depending on the value of δ . Therefore, it may be too rigid since it is not able to cover mixed extremal dependence classes in the two dimensions.

We propose the following space-time model:

$$X(s, t) = R(t)^\delta W(s, t)^{1-\delta}, \quad \delta \in [0, 1], \quad (4)$$

where the processes $R(t)$ and $W(s, t)$ are mutually independent with standard Pareto marginal distribution. Making R depend on t provides more flexibility to the model, allowing to get different extremal dependence classes in space and time, as shown in [Section 2.3](#). The marginal distribution of $X(s, t)$ is given by

$$G(x) = \begin{cases} 1 - [\delta/(2\delta - 1) x^{-1/\delta} - (1 - \delta)/(2\delta - 1) x^{-1/(1-\delta)}] & \text{for } \delta \neq 0.5, \\ 1 - x^{-2}[2 \log(x) + 1] & \text{for } \delta = 0.5. \end{cases} \quad (5)$$

An alternative formulation of model (4) can be obtained by taking the logarithm

$$\tilde{X}(s, t) = \delta \tilde{R}(t) + (1 - \delta) \tilde{W}(s, t), \quad (6)$$

where $\tilde{X}(s, t) := \log\{X(s, t)\}$, $\tilde{R}(t) := \log\{R(t)\}$ and $\tilde{W}(s, t) := \log\{W(s, t)\}$. In such case the marginal distributions of $\tilde{R}(t)$ and $\tilde{W}(s, t)$ are standard exponential distributions and the marginal distribution of $\tilde{X}(s, t)$ is known as hypo-exponential or general Erlang distribution (Johnson et al., 1994, p. 552). The formulation (6) preserves the extremal dependence structure of (4), but it is computationally more stable, making it preferable for simulation and parameter estimation.

The representation (6) shares some similarities with the model presented in Majumder and Reich (2023), namely

$$\tilde{X}_t(s) = \delta(t) \tilde{R}_t(s) + (1 - \delta(t)) \tilde{W}_t(s), \quad \delta(t) \in [0, 1],$$

where $\tilde{R}_t(s)$, $t = 1, \dots$, are independent copies of an AD spatial process, and $\tilde{W}_t(s)$, $t = 1, \dots$, are independent copies of an AI spatial process. However, the authors of the aforementioned paper primarily focused on the spatial extremal dependence. They allowed for the possibility that this spatial dependence may not be stationary in time by varying the delta function. In contrast, the present study posits that the extremal dependence is driven by two processes, denoted $\tilde{R}(t)$ and $\tilde{W}(s, t)$, which do exhibit time and space-time dependence.

Before illustrating the extremal dependence properties of the model (4), we highlight its inherent asymmetry. The current definition uses two distinct stochastic processes to model temporal dependence and one to model spatial dependence. An alternative is

$$X(s, t) = R(s)^\delta W(s, t)^{1-\delta}, \quad (7)$$

where more flexibility is allocated to the spatial dimension. Our selection of (4) is motivated by its application in our real-data analysis. However, studying the extremal dependence properties of the alternative model would not introduce additional complexity if we carefully invert the roles of the spatial and temporal dimensions. Table S2 in the Supplementary material summarizes the dependence properties of models derived from equation (7).

2.3. Dependence properties of the model

In principle, both $R(t)$ and $W(s, t)$ in (4) can be AI or AD stochastic processes. This results in four different models for $X(s, t)$ with different extremal dependence, which are summarized in Table 1. The Table shows the extremal dependence for pairs $X(s_1, t_1)$, $X(s_2, t_2)$ in space (i.e., for $s_1 \neq s_2$, $t_1 = t_2$), in time (i.e., for $s_1 = s_2$, $t_1 \neq t_2$) and in space-time (i.e., for $s_1 \neq s_2$, $t_1 \neq t_2$), for different values of the parameter δ .

For a detailed exposition of the proofs in the space-time case, the reader is referred to the appendices, which follow an approach similar to that of Engelke et al. (2019). In

Model	$R(t)$	$W(s, t)$	$\delta > 0.5$	$\delta = 0.5$	$\delta < 0.5$
1	AI	AD	AD in space AI in time AI in space-time	AD in space AI in time AI in space-time	AD in space AD in time AD in space-time
2	AD	AI	AD in space AD in time AD in space-time	AI in space AI in time AI in space-time	AI in space AI in time AI in space-time
3	AI	AI	AD in space AI in time AI in space-time	AI in space AI in time AI in space-time	AI in space AI in time AI in space-time
4	AD	AD	AD in space AD in time AD in space-time	AD in space AD in time AD in space-time	AD in space AD in time AD in space-time

Table 1: The four possible combinations for $R(t)$ and $W(s, t)$ and the resulting extremal dependence for pairs $[X(s_1, t_1), X(s_2, t_2)]$ in space, in time and in space-time, for different values of the parameter δ . These statements are supported by proof in [Appendix A](#) and [Appendix B](#).

particular, [Appendix A](#) contains the proofs of the results for pairs in time and space-time, while [Appendix B](#) refers to pairs in space.

With the exception of Model 4, all other models are characterized by two different extremal dependence configurations in space and time. The selection between these configurations is dependent on the value of the parameter δ . In particular, δ controls which of the two components, $R(t)$ or $W(s, t)$, dominates in the mixture and leads the extremal dependence. This allows for the comparison and testing of a pair of scenarios specific to each model. When $\delta > 0.5$, $X(s, t)$ belongs to the same extremal dependence class as $R(t)$ for spatio-temporal pairs and also for temporal pairs. However, for $t = \bar{t}$ fixed, $R(\bar{t})$ is a single random variable, so it is exactly dependent for spatial pairs, regardless of the dependence class of $R(t)$; then, these pairs are always AD when $\delta > 0.5$. On the other hand, when $\delta < 0.5$, $W(s, t)$ dominates the mixture and controls the extremal dependence for all the pairs of $X(s, t)$. When $\delta = 0.5$, the pairs are AI if they are also AI for at least one value of $\delta \neq 0.5$, otherwise they are AD.

This subsection concludes by introducing two specifications of processes, $R(t)$ and $W(s, t)$, that we use in our numerical examples. They are derived by transforming two other underlying processes, denoted by $R^*(t)$ and $W^*(s, t)$.

The most prevalent and extensively utilized class of AI processes is that of Gaussian processes. Here we consider Gaussian processes with underlying correlation function $\rho(l_1, l_2)$ for two generic time or space-time locations l_1 and l_2 . The Gaussian processes satisfy (2) with $\eta(l_1, l_2) = 1 + \rho(l_1, l_2)/2$ ([Sibuya, 1960](#); [Ledford and Tawn, 1996](#)), so that $\eta(l_1, l_2) < 1$ (asymptotic independence) whenever $\rho(l_1, l_2) < 1$. Their usefulness as a model for $R(t)$ or $W(s, t)$ is motivated by the wealth of examples of parametric correlation functions and by the relative simplicity of the simulation.

On the other hand, max-stable processes are an important class of AD processes. However, their simulation and inference are computationally prohibitive in high dimensions (see, for instance, [Huser and Wadsworth, 2020](#)).

The class of Student's t processes ([Røislien and Omre, 2006](#)) provides a manageable alternative. Student's t processes with $\nu > 0$ degrees of freedom are defined as zero mean and unit variance Gaussian processes, with correlation function $\rho(l_1 - l_2)$, divided by the square root of a Gamma random variable, with shape parameter $\nu/2$ and rate parameter $\nu/2$. They are AD processes ([Chan and Li, 2008](#)) and converge to the Gaussian limit as $\nu \rightarrow \infty$.

Therefore, in the following we consider two stationary processes, which can be Gaussian or Student's t processes with ν degrees of freedom, named $R^*(t)$ and $W^*(s, t)$. Both processes are identified by two positive definite functions $\rho_{R^*}(k; \phi)$, $k \in \mathbb{R}$, and $\rho_{W^*}(h, k; \psi)$, $(h, k) \in \mathbb{R}^2 \times \mathbb{R}$, where ϕ and ψ are two sets of parameters. The transformations

$$\begin{aligned} R(t) &= 1/[1 - F_{R^*}(R^*(t))], \\ W(s, t) &= 1/[1 - F_{W^*}(W^*(s, t))] \end{aligned} \tag{8}$$

where F_{R^*} and F_{W^*} are the marginal distribution functions of $R^*(t)$ and $W^*(s, t)$, cause $R(t)$ and $W(s, t)$ to marginally follow a standard Pareto distribution and preserves the extremal dependence class of the original processes.

2.4. A model for the marginals

The model specified by (4) is employed as a copula to describe the extremal dependence of the data $Y(s, t)$. To model extreme values of the observation $Y(s, t)$, we employ a Peaks Over Thresholds (POT) approach ([Davison and Smith, 1990](#); [Eastoe and Tawn, 2009](#)). This approach involves fixing a threshold, denoted by $\mu(s, t)$, which represents the p -quantile of the distribution of $Y(s, t)$ at location s and time t , and using a generalized Pareto distribution as the stochastic model for the exceedances over the threshold.

More precisely, it is assumed that $X(s, t)$, as defined in (4), is a stationary process and G is its marginal distribution, as defined in (5). Then, the values of the process $X(s, t)$ are transformed into

$$Y(s, t) = Q_{s,t}(G(X(s, t))), \tag{9}$$

where

$$Q_{s,t}(u) = \begin{cases} \mu(s, t) & \text{for } 0 < u \leq p, \\ \mu(s, t) + \sigma \left[\left[1 - (u - p)/(1 - p) \right]^{-\xi} - 1 \right] / \xi & \text{for } p < u < 1, \end{cases} \tag{10}$$

with $0 < p < 1$. Note that although the parameters σ and ξ could theoretically depend on space or time, we assume here that they are constant based on the real data example in Section 4. Also note that the censoring scheme in (10) does not affect the values of the coefficient χ in (1) and of its sub-asymptotic version $\chi(u)$ with $u > p$.

3. Estimation method

Our final stochastic model for the extreme values of $Y(s, t)$ is the result of composing the copula model (8) and (4) and the marginal model (9). In the following, the set of parameters of the copula model is denoted as $\theta_D := (\phi, \psi, \delta)$ and the set of marginal parameters is given by $\theta_M = (\sigma, \xi)$.

The estimation of the parameters of scale mixture models is typically accomplished through two sequential steps (see the works of [Huser et al. \(2017\)](#), as well as of [Huser and Wadsworth \(2019\)](#)), that we describe shortly to highlight the complexity of adopting it in our case.

1. The first step deals with the marginal parameters θ_M of the cumulative distribution function (CDF) derived from (9)

$$F_{s,t}(y) = \begin{cases} p + (1-p) \left[1 - (1 + \xi(y - \mu(s, t))/\sigma)_+^{-1/\xi} \right] & \text{for } y > \mu(s, t), \\ p & \text{for } y \leq \mu(s, t), \end{cases}$$

where $(a)_+ = \max(0, a)$. The estimation of θ_M can be based on the maximization of the independence likelihood ([Varin et al., 2011](#)). This approach is used in our numerical examples.

2. In the second step, it is assumed that for the observations above $\mu(s, t)$ the process $Y(s, t)$ has the same copula of $X(s, t)$. A likelihood-based inference approach for estimating θ_D requires evaluating the joint distribution of $X(s_i, t_i)$, $i = 1, \dots, n$, where n is the number of space-time observations.

With $X_i = X(s_i, t_i)$, $R_i = R(t_i)$, $W_i = W(s_i, t_i)$ we can write the CDF of $\mathbf{X} = (X_1, \dots, X_n)$ as

$$\begin{aligned} F_{\mathbf{X}}(x_1, \dots, x_n) &= \mathbb{P}(X_1 \leq x_1, \dots, X_n \leq x_n) \\ &= \mathbb{P}(R_1^\delta W_1^{1-\delta} \leq x_1, \dots, R_n^\delta W_n^{1-\delta} \leq x_n) \\ &= \mathbb{P}\left(W_1 \leq x_1^{1/(1-\delta)} R_1^{-\delta/(1-\delta)}, \dots, W_n \leq x_n^{1/(1-\delta)} R_n^{-\delta/(1-\delta)}\right) \\ &= \int_0^\infty \dots \int_0^\infty F_{\mathbf{W}}\left(x_1^{1/(1-\delta)} r_1^{-\delta/(1-\delta)}, \dots, x_n^{1/(1-\delta)} r_n^{-\delta/(1-\delta)}\right) \times \\ &\quad f_{\mathbf{R}}(r_1, \dots, r_n) dr_1 \dots dr_n \end{aligned}$$

and the density function of \mathbf{X} as

$$\begin{aligned} f_{\mathbf{X}}(x_1, \dots, x_n) &= \frac{1}{(1-\delta)^n} \prod_{i=1}^n x_i^{\delta/(1-\delta)} \times \\ &\quad \int_0^\infty \dots \int_0^\infty f_{\mathbf{W}}\left(x_1^{1/(1-\delta)} r_1^{-\delta/(1-\delta)}, \dots, x_n^{1/(1-\delta)} r_n^{-\delta/(1-\delta)}\right) \times \\ &\quad \prod_{i=1}^n r_i^{-\delta/(1-\delta)} f_{\mathbf{R}}(r_1, \dots, r_n) dr_1 \dots dr_n, \end{aligned}$$

where $F_{\mathbf{W}}$ and $f_{\mathbf{W}}$ indicate the CDF and the density of $\mathbf{W} = (W_1, \dots, W_n)$ and $f_{\mathbf{R}}$ the density of $\mathbf{R} = (R_1, \dots, R_n)$. In general, there is no analytical formula for $F_{\mathbf{X}}$ or $f_{\mathbf{X}}$ and the evaluation of the multiple integral is the core of the computational task. Note that in the spatial case of the model (3), the previous formulas reduce to a one-dimensional integral (see [Huser and Wadsworth, 2019](#), Eq. (15)-(16)). On the other hand, the computation of bivariate distribution functions for model (4) involves at least a double integral (when $n = 2$), making parameter estimation still infeasible even when inference is based on pairwise likelihoods as in [Huser and Davison \(2014\)](#).

Notwithstanding the challenges associated with implementing a likelihood-based approach for estimating θ_D , it is noteworthy that simulating a large number of spatiotemporal datasets from the copula model is comparatively easy and fast. In the following, we propose an estimation of the parameters of interest based on a simulated approach inspired by the Neural Bayes estimators ([Richards et al., 2024](#); [Sainsbury-Dale et al., 2024](#)).

The idea is to choose, or randomly generate, a dense configuration of values covering the entire parameter space, or a reasonable subset of it. For each parameter value, a space-time dataset is then simulated. The implicit mapping that connects data and parameters is estimated by a neural network. The same network can then be used to predict parameter values from datasets that are similar, in terms of parameter space, to those used for its training. The variability of these point estimates is typically evaluated through a bootstrap procedure.

A major difference, compared to the Neural Bayes Estimators, is that we use appropriately chosen summary statistics as input of the neural networks, instead of letting the network extract them from the datasets. A similar approach has been implemented by [Gerber and Nychka \(2021\)](#) in the geostatistical context. Although the optimality of the choice of statistics is not guaranteed, this leads to less memory usage and faster network training, allowing the space-time dimensionality to be considerably increased. In particular, we employ the empirical pairwise coefficient $\hat{\chi}(u)$, which has been previously used as input of a neural network by [Ahmed et al. \(2022\)](#). In practice, the data are divided into N independent blocks of space- and time-dependent observations, so the coefficient is computed, for a specific lag in space and time, as an average over the blocks. For instance, in the data application (Section 4) each block corresponds to one year. We define the empirical coefficient, for the block-specific observations $y_{1,i}, y_{2,i}$ of the generic pair $Y_1 = Y(s_1, t_1), Y_2 = Y(s_2, t_2)$, as

$$\hat{\chi}(u) = \frac{\sum_{i=1}^N \mathbb{1}(y_{1,i} > \hat{F}_1^{-1}(u), y_{2,i} > \hat{F}_2^{-1}(u))}{N(1-u)}, \quad (11)$$

where $\hat{F}_1^{-1}(u)$ and $\hat{F}_2^{-1}(u)$ are the estimated quantiles of order u for the locations s_1 and s_2 , with $u > p$ in (10). Moreover, we compute the mean of $\hat{\chi}(u)$ for all the pairs (s_1, t_1) and (s_2, t_2) lying at m_1 different ranges of spatial distances and m_2 temporal lags, resulting in a grid of $m_1 \times m_2$ values in $[0, 1]$. This is done for $u \in \{0.90, 0.95, 0.99\}$, leading to three different grids meant to cover the sub-asymptotic dynamics of the spatio-temporal dependence of the data. In the data application presented in Section 4, $m_1 = m_2 = 8$, with the longest distance in the grids set at 34 km, i.e. the half of the maximum distance of

Algorithm 1 Neural estimation method for θ_D

Simulation

1. Generate many parameter values θ_D^* uniformly on the parameter space
2. Simulate a dataset y^* from the model for each parameter value θ^*
3. Summarize each dataset y^* through some statistics z^*

Point estimation

4. Learn the map $g(\cdot)$ that connects θ_D^* to the statistics z^* using neural networks
 5. Use the map to predict a value of θ_D from the statistics computed on the observed dataset, z^o . The predicted value $\hat{\theta}_D = g(z^o)$ is the neural estimate
-

the observed locations, and the time lags that range from 0 to 7 days, since we assume the correlation to be negligible for higher distances. Note that (11) is the empirical version of (1) for a finite threshold, even though the first is defined for the process $Y(s, t)$, in the scale of the observed data, while the second refers to the copula process $X(s, t)$. Indeed, the marginal transformation linking the two processes does not affect the values of this coefficient.

In the network training, a two-dimensional convolution (Lopez Pinaya et al., 2020) is applied to the $m_1 \times m_2$ grids of $\hat{\chi}(u)$'s, treating each of the three grids as a channel, as if they were the three RGB colours intensity of an image (LeCun et al., 2015). The result is then passed through few dense layers, resulting in an output vector corresponding to the values of the parameters. The loss function to be minimized by the network is the mean absolute error. In our setting, the validation set consists of 20% of the input data. The neural network is built and trained using the R package `keras3` (Kalinowski et al., 2024) an interface to Keras, a high-level neural networks API. The training takes about one minute on a standard laptop, using the Root Mean Square Propagation (RMSprop) optimization algorithm and 40 epochs for data split into batches of size 128. For more details on the implementation of the convolutional layers and the estimation algorithm, see the Keras page <https://keras.io>.

The amount of input data for training and testing a neural network is a crucial parameter and there is no general rule. This amount would depend on the number of parameters, the architecture of the neural network, and the optimization algorithm used. In this study, an empirical approach is adopted, wherein the model is trained on datasets of increasing size, and the validation performance is observed. For our specific numerical examples (Section 4), we have seen that if we randomly generate $K = 30\,000$ parameter vectors on Θ_D , we get stable results. For each of these parameter values, a dataset is simulated with the same spatial locations and time periods as the observed one. Each dataset is then summarized by the statistics described above. This simulation takes about 320 minutes on a 2.3 GHz machine with 32 cores and 30 GB of memory. We have also experimented that increasing K up to 70 000 does not change significantly the validation performance.

The estimation method described above is summarized in Algorithm 1. An R code implementing it is available on request from the authors. Note that, once the network is trained (point 1. to 4.), it can be applied to other datasets, similar to the original one in terms of structure and parameter space, to get parameter estimates very quickly (Sainsbury-Dale et al., 2024). Moreover, the employed statistics focus on the joint tail (above 0.90-quantiles) of the data distribution, without giving the network any information on its bulk; in this way, we are operating an implicit censoring on the data, without the need to adapt the network to a censoring scheme, as in Richards et al. (2024).

The variability of the point estimates for both θ_D and θ_M is evaluated through a parametric bootstrap approach: once we get the neural estimate $\hat{\theta}_D$, we use it to simulate $B = 400$ datasets from $X(s, t)$, and apply the same network to each dataset, getting estimates $\hat{\theta}_D^b$, for $b = 1, \dots, B$; moreover, we transform each dataset to the $Y(s, t)$ scale through (9), using the maximum (independence) likelihood estimate $\hat{\theta}_M$, and we evaluate $\hat{\theta}_M^b$, for $b = 1, \dots, B$. We can then compute bootstrap confidence intervals as percentile intervals based on the univariate distribution of the estimates for each parameter.

4. Numerical examples

4.1. Rainfall data

The models described in Section 2 are applied to a dataset of daily rainfall collected between 1999 and 2018 in the North Brabant province of the Netherlands. The dataset, already studied by Bortot and Gaetan (2024), was downloaded from the European Climate Assessment (ECA) and Dataset website (<https://www.ecad.eu>) and contains data collected over 30 stations, after discarding those with missing data. Moreover, we focus here on spring months (March, April, May) to avoid seasonality. This leads to 20 blocks (each corresponding to one year) of 92 observations for each station. The data are assumed to be time-dependent within each year and independent between years. Figure 1 shows the location of the 30 stations within the Netherlands. The relatively small size and the geographic homogeneity of the region support the hypothesis of strong spatial dependence of climate events (such as rainfall) within it, although this dependence is not necessarily persistent as the magnitude of the events becomes more extreme.

Figure 2 displays the empirical estimates of the coefficient $\chi(u)$, defined in (11), on the North Brabant dataset, for $u \in \{0.90, 0.95, 0.99\}$, for pairs at different spatial distances, averaging across all time periods, and for pairs at different temporal lags, averaging across all sites. The shaded areas represent 95% pointwise confidence intervals obtained by 200 replications of a block bootstrap. Although empirical estimates decrease with spatial and temporal distances, their limit as u increases appears to be positive in the first case and zero in the second case. This may be an evidence of asymptotic dependence in space and asymptotic independence in time.

North Brabant stations



Figure 1: Location of the 30 stations in the North Brabant province of the Netherlands.

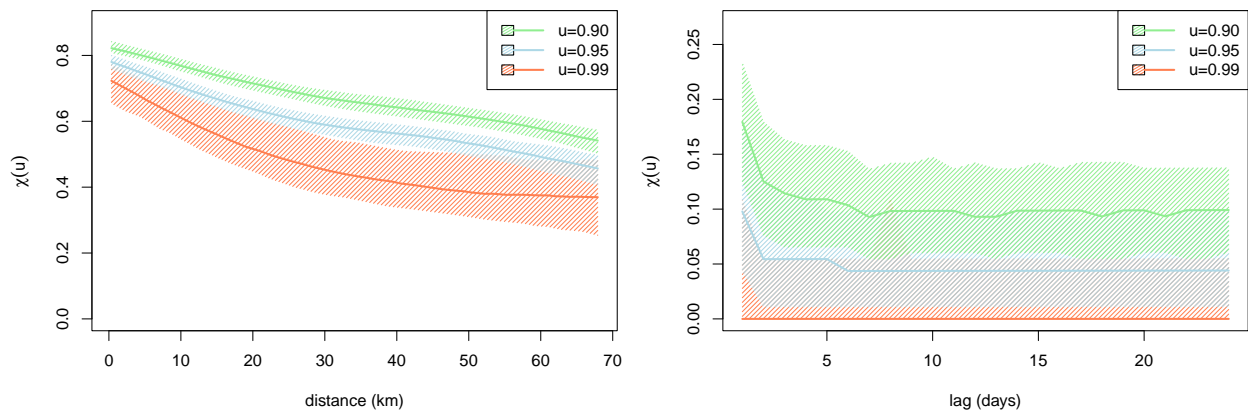


Figure 2: For the North Brabant rainfall data, empirical estimates of $\chi(u)$, $u = 0.90, 0.95, 0.99$, for pairs of observations at increasing spatial distances (left) and temporal lags (right). The shaded areas represent approximate 95% confidence regions based on a stationary bootstrap procedure.

4.2. Space-time model for rainfall data

Bortot and Gaetan (2024) study the same data, although focusing on different months, and compare models with various space-time extremal dependence, concluding that the process underlying the rainfall data in the North Brabant province is AI in time and AD in space. This setting, which seems to be confirmed by exploratory analysis on our data (see Figure 2), is possible only under Model 1 and Model 3 (see Table 1), so we focus on these two configurations. Note that the value of δ has a different interpretation in the two models: Model 1 is always AD in space and could be AI or AD in time and space-time, depending on

δ ; Model 3 is always AI in time and space-time and could be AI or AD in space, depending on δ .

In Model 1 and Model 3, $R(t)$ is chosen to be asymptotically independent, more precisely, $R^*(t)$ is a Gaussian process with zero mean and unit variance, with correlation function $\rho_{R^*}(k; \phi) = \exp(-k/\phi)$, for temporal lag k .

The process $W(s, t)$ should be AD in Model 1 and AI in Model 3. In both cases, we again follow (8), where $W^*(s, t)$ is a Gaussian or Student's t process with $\nu = 1$ degrees of freedom, respectively. The parameter ν could also be estimated, but we fix its value at 1 to limit the number of parameters. Moreover, as $\nu \rightarrow \infty$, the Student's t process tends to a Gaussian process, i.e., an AI process. Thus, setting a low value for ν helps to make a clear distinction between AI and AD processes. We also assume that the Gaussian process (possibly divided by a random variable to get a Student's t) has a space-time correlation function, namely $\rho_{W^*}(h, k; \psi) = [1 + (\|h\|/\psi_1)^2]^{-1} \exp(-k/\psi_2)$, for spatial lag h and temporal lag k , which is a separable version of the space-time correlation function in Gneiting (2002). Some results with a different correlation function are presented in the Supplementary material. The separability in the correlation function implies a parsimonious parameterization and speeds up the simulation of the processes. Note that, even if $W^*(s, t)$ is a Gaussian process with separable covariance function, this is not the case for the non linearly transformed process $W(s, t)$, when its covariance function exists.

Model 1 and Model 3 share the same set of copula parameters, $\theta_D := (\delta, \phi, \psi_1, \psi_2)$, but the role and interpretation of the values is specific to each model, especially for the δ parameter.

The training of the neural network involved, for both Model 1 and Model 3, 30 000 simulated datasets with the same 30 spatial location and time dimension of the observed one: 20 years \times 92 days. For each dataset, a parameter value is uniformly generated on the following sets: (0, 1) for δ , (0, 2.5) for ϕ , (4, 16) for ψ_1 , (0, 2.5) for ψ_2 . For the parameters ϕ , ψ_1 and ψ_2 , the boundaries help to reduce the number of simulations needed to cover the four-dimensional parameter space. To set the boundaries, we checked that the resulting parameter space encompasses a range of values of $\chi(0.9)$, evaluated by Monte Carlo method at the observed distances in space and time, consistent with the range of the empirical values reported in Figure 2.

To model the marginal distribution of the data, we follow the POT approach described in 2.4. In particular, we assume that the thresholds $\mu(s, t) = \mu(s)$ in (10) depend only on the spatial location s . This assumption is based on the fact that we restrict the analysis to the spring months, for which we assume temporal stationarity of the data. The value of $\mu(s)$ is preliminarily estimated by quantile regression for the 0.90-quantile with spatial coordinates as covariates. In addition, following Bortot and Gaetan (2024), we assume that the distribution of exceedances is invariant with spatial location, resulting in a scale parameter σ and a shape parameter ξ that are constant over the whole province of North Brabant. In Section S3 in the Supplementary material, a justification for this choice is provided by fitting site-specific GPD models to the data and showing that, for all stations, the confidence intervals include the values of σ and ξ estimated on the overall data. This could be intuitively explained by the small size of the studied spatial domain and by its

geographical regularity.

4.3. Simulated data

The goal of the following simulation study is not to be exhaustive but rather to understand how a neural network-based estimation method for the copula model parameters, described in Section 3, might be able to infer the different classes of extremal dependence and to produce at least experimentally consistent estimates on a real-world example. In this regard, the spatial configuration was determined by selecting the pattern of sites in North Brabant with an equal number of observations over time. Furthermore, the models for temporal and spatio-temporal dependence remain the same as in Section 4.2.

Because of its relevance to the determination of the extremal dependence, we focus first on the estimation of δ . For each value of δ in $\{0.1, 0.2, \dots, 0.9\}$, 200 data sets are generated from Models 1 and 3. In this experiment, we keep the true values of the other parameters constant and equal to the estimates displayed in Table 2, i.e. $\phi = 0.874, \psi_1 = 9.107, \psi_2 = 0.328$ for Model 1, $\phi = 1.045, \psi_1 = 10.045, \psi_2 = 0.377$ for Model 3. The results, for δ only, are shown in Figure 3. For simplicity, the results for the other parameters are not shown here, even though they are also estimated jointly with δ .

The estimation method seems to work well enough to discriminate correctly between values smaller or greater than 0.5, confirming that inference on δ is a viable means of determining the extremal dependence of the data, within the possibilities of each model (see Table 1). The boxplots for an analogue simulation study referring to Model 2 and Model 4 are reported in Figure S1 in the Supplementary material.

A second experiment, shown in Figure 4 and Figure 5, focuses on the estimation of the other dependence parameters ψ_1, ψ_2 and ϕ . Figure 4 displays the boxplots of the estimated values for four configurations (A, B, C, D) of δ, ψ_1 (scale of the spatial correlation of the Gaussian process $W^*(s, t)$), ψ_2 (scale of the temporal correlation for the same process) and ϕ (scale of the temporal correlation of the Gaussian process $R^*(t)$). The configurations are

- A: $R(t)$ leads the mixture ($\delta = 0.7$), with $\psi_1 = 13, \psi_2 = 0.7$ and $\phi = 0.7$;
- B: $W(s, t)$ leads the mixture ($\delta = 0.3$), with $\psi_1 = 13, \psi_2 = 0.7$ and $\phi = 0.7$;
- C: $R(t)$ leads the mixture ($\delta = 0.7$), with $\psi_1 = 7, \psi_2 = 0.7$ and $\phi = 0.7$;
- D: $W(s, t)$ leads the mixture ($\delta = 0.3$), with $\psi_1 = 7, \psi_2 = 0.7$ and $\phi = 0.7$.

In all cases, spatial locations, time periods and number of independent replication (i.e., number of years) are fixed as the ones in the dataset. For simplicity, the values of ψ_2 and ϕ are the same in all configurations; note that other values are explored in Figure 5. While the spatial dependence parameter ψ_1 is well estimated for both Model 1 and Model 3 (the corresponding boxplots referring to Model 2 and Model 4 are reported in Figure S2 in the Supplementary material), the estimation of the temporal dependence parameters is more

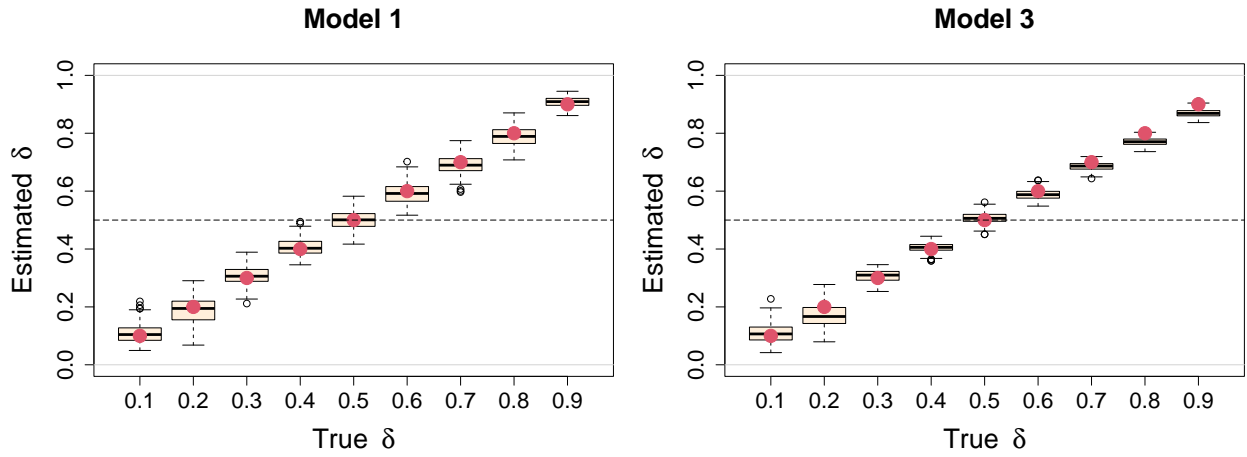


Figure 3: True (red points) and estimated (boxplots) values of δ on 200 independently simulated datasets, for Model 1 (left) and Model 3 (right).

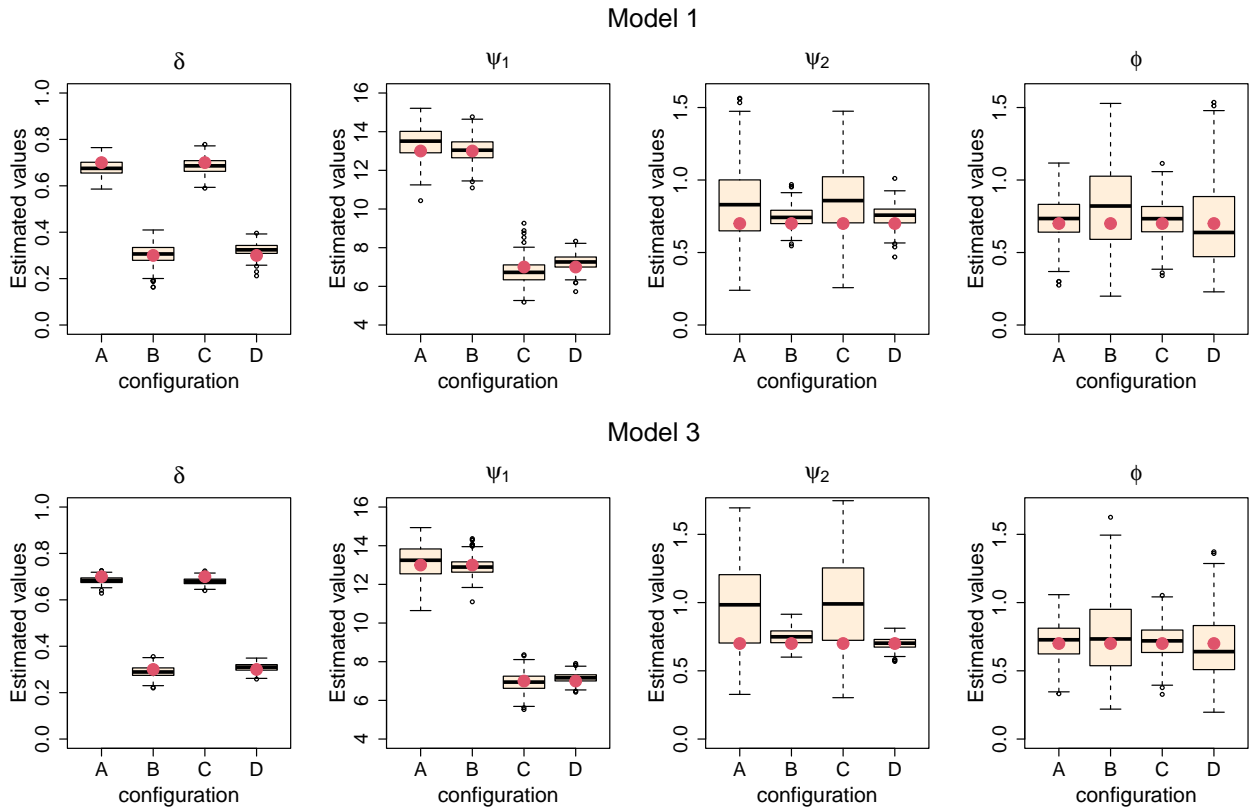


Figure 4: Boxplots of the estimated values for $\delta = 0.7$ (A,C) or $\delta = 0.3$ (B,D), $\psi_1 = 13$ (A,B) or $\psi_1 = 7$ (C,D), $\psi_2 = 0.7$ and $\phi = 0.7$ (red points) obtained on 400 simulated datasets from Model 1 and Model 3.

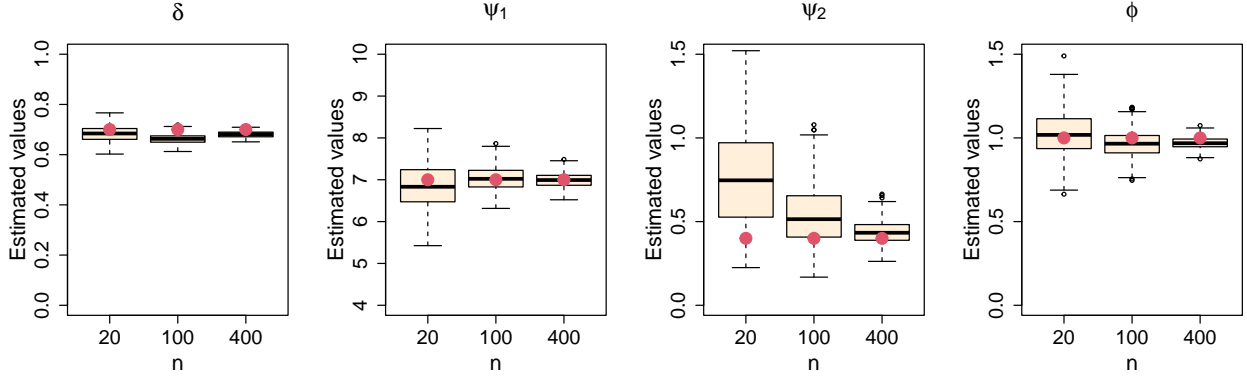


Figure 5: Boxplots of estimated values for $\delta = 0.7$, $\psi_1 = 7$, $\psi_2 = 0.4$ and $\phi = 1$ (red points) obtained on 400 datasets simulated from Model 1, with N spatio-temporal independent replications in each dataset.

difficult in configurations A and C (for ψ_2) and B and D (for ϕ), i.e. when the corresponding process is dominated by the other in the mixture.

Finally, we explore the consistency of the estimation method for ψ and ϕ in Figure 5; here $\delta = 0.7$, and the identifiability of ψ_2 is even more difficult because its value is lower than that of ϕ , the time dependence parameter of the dominating process. Indeed, when we fix N , the number of independent replications of the space-time dependent data, at 20, as in Figure 4, the estimation of ψ_2 is poor. However, as we increase N to 100 and 400, all the parameters are correctly identified by the estimation method presented in Section 3.

4.4. Results for real data application

The estimated values of the parameters and the bootstrap confidence intervals are reported in Table 2. In particular, $\hat{\delta} > 0.5$ for both Model 1 and Model 3. Therefore, both models support the conclusion that rainfall data in the North Brabant province are asymptotically dependent in space and asymptotically independent in time (see Table 1), which is consistent with the findings of Bortot and Gaetan (2024) and with the preliminary analysis shown in Figure 2.

Model	Dependence parameters (θ_D)				Marginal parameters (θ_M)	
	δ	ϕ	ψ_1	ψ_2	σ	ξ
1	0.577	0.874	9.107	0.328	46.34	0.114
	(0.519,0.634)	(0.691,1.127)	(8.367,10.112)	(0.176,0.588)	(37.97,62.19)	(-0.026,0.211)
3	0.631	1.045	10.045	0.377	46.34	0.114
	(0.585,0.645)	(0.827,1.297)	(9.703,11.212)	(0.204,0.632)	(38.13,62.07)	(-0.026,0.204)

Table 2: Estimated values and 0.90 bootstrapped confidence intervals, in parentheses, for the parameters in θ_D and θ_M .

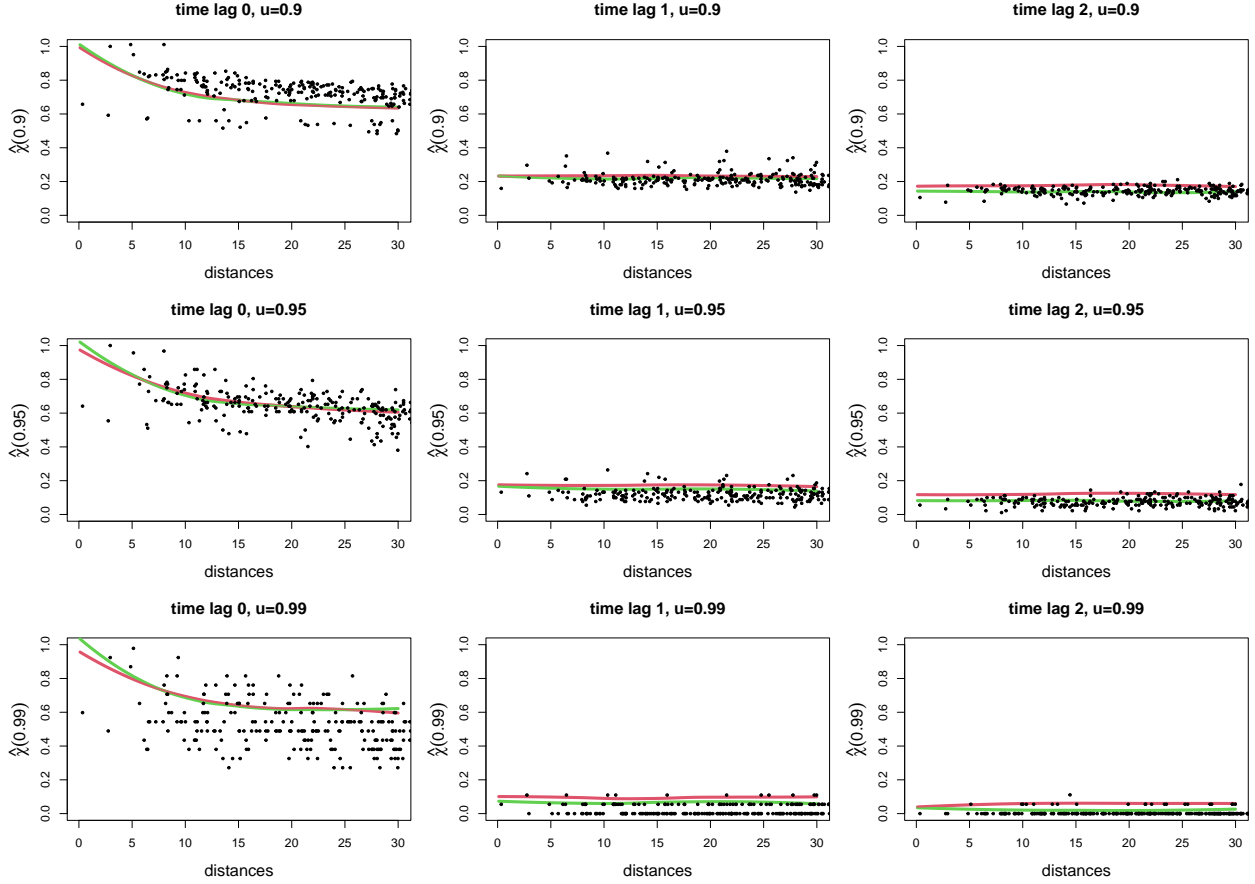


Figure 6: Values of $\chi(u)$ for different spatial distances and temporal lags, derived from the estimated Model 1 (red lines), from the Model 3 (green lines) and the empirical ones for each pair of stations (dots).

Figure 6 shows the empirical pairwise coefficient $\hat{\chi}_{1,2}(u)$, as defined in (11), for pairs (Y_1, Y_2) at different distances in space and time and for $u \in \{0.90, 0.95, 0.99\}$. The dots represent the empirical coefficients observed in the dataset, while the lines are smoothed estimates from the two models, evaluated by simulation. Both the models are able to capture the decay of joint tail probabilities, characterized by the persistence of positive values in space, symptom of asymptotic dependence (first column), and by values rapidly going to zero for pairs at time lag 1 or 2, that are asymptotically independent (second and third columns). Figure S3 in the Supplementary material shows the same plot for a model defined with correlation functions different from those presented in 4.2.

It is not straightforward to determine which model best fits the data from Figure 6. To formally do so, we perform a likelihood-free model selection based on cross validation. Since the dataset includes twenty years of daily observation, and we assume independence and stationarity among years, we split it into a 15-years block and a 5-years block, randomly sampled. The grids of empirical $\hat{\chi}$ described in Section 3 are computed separately on the two blocks. The ones computed on the 15-years block are used to get parameter estimates for each model from the neural network, and 500 5-years datasets are simulated to get a

Monte Carlo estimate of the grids, to be compared with those computed on the 5-years left-out block, through the Root Mean Squared Error (RMSE). This procedure is repeated iteratively 50 times. The resulting RMSE is equal to 0.066 for Model 1 and to 0.064 for Model 3, indicating a slight preference for the latter.

Another diagnostic measure that we adopt, similarly to [Bacro et al. \(2020\)](#), is

$$\chi_{s_i;k}^*(u) := \mathbb{P} \left(Y(s_j, t) > \widehat{F}_j^{-1}(u), \forall s_j \in \partial s_i \mid Y(s_i, t - k) > \widehat{F}_i^{-1}(u) \right)$$

where ∂s_i is the set of the four nearest neighbors of site s_i , $i = 1, \dots, 30$ and $\widehat{F}_i^{-1}(u)$ and $\widehat{F}_j^{-1}(u)$ are the estimated quantiles of order u for the locations s_i and s_j . This allows to evaluate the performance of the models with respect to higher-dimensional extremal dependence in space and time, while the parameter estimation relies on pairwise information only, see (11). The empirical estimates of $\chi_{s_i;k}^*(u)$, $\widehat{p}_i(k, u)$, for $k \in \{0, 1, 2\}$ and $u \in \{0.90, 0.95\}$, are compared with parametric bootstrap estimates $\widetilde{p}_i^{(j)}(k, u)$, for $j = 1, \dots, 1000$, through the site-specific RMSE

$$\text{RMSE}_i(k, u) = \left\{ \frac{\sum_{j=1}^{1000} (\widetilde{p}_i^{(j)}(k, u) - \widehat{p}_i(k, u))^2}{1000} \right\}^{1/2}$$

and the total mean $\text{RMSE}(k, u) = \sum_{i=1}^{30} \text{RMSE}_i(k, u)/30$, which is reported in [Table 3](#). Model 3 seems to perform better than Model 1 on the multivariate spatial dependence for neighbors at the same time periods ($k = 0$) and higher quantile ($u = 0.95$), while the performance of the two models is similar in the other settings. [Table S1](#) in the Supplementary material contains the same measures for a model defined with correlation functions different from those presented in [4.2](#).

Model	$k = 0$		$k = 1$		$k = 2$	
	$u = 0.90$	$u = 0.95$	$u = 0.90$	$u = 0.95$	$u = 0.90$	$u = 0.95$
1	0.116	0.138	0.025	0.027	0.027	0.028
3	0.111	0.109	0.028	0.030	0.027	0.030

Table 3: $\text{RMSE}(k, u)$ between empirical estimates of $\chi_{s_i;k}^*(u)$ and estimates from Model 1 and Model 3 (see [Table 1](#)).

[Figure 7](#) shows the distribution of thresholds exceedances observed in the rainfall dataset. The thresholds $\mu(s)$ are the 0.90-quantiles at each station, estimated via quantile regression. The dashed blue line is the theoretical GPD density with the parameter values set as the maximum likelihood estimate. The estimated values and the bootstrap confidence intervals for the scale parameter σ and for the shape parameter ξ are reported in [Table 2](#).

Exceedances distribution

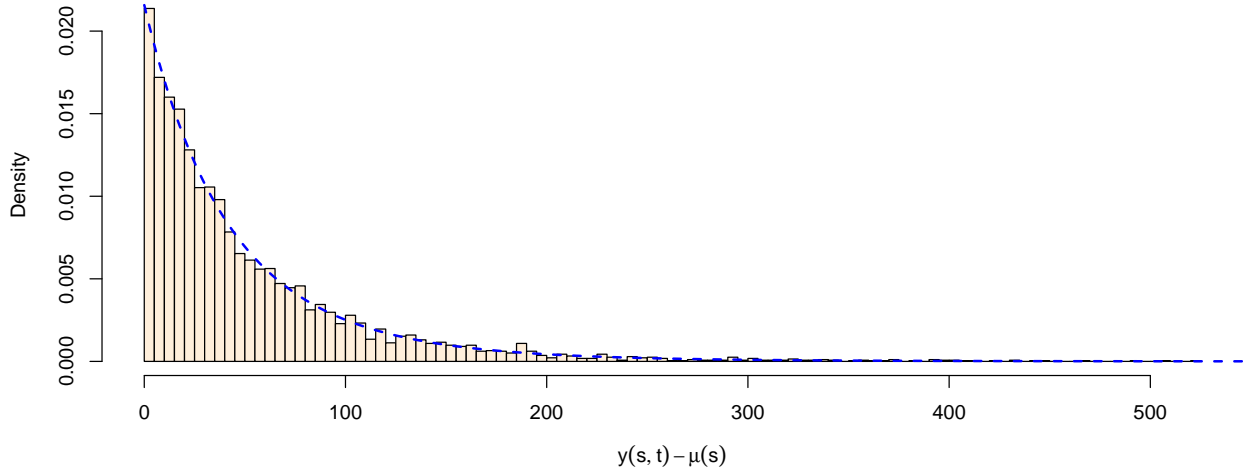


Figure 7: Observed right tail (threshold exceedances) of the marginal distribution. The dashed blue line is the GPD density with parameters equal to the maximum likelihood estimates $\hat{\sigma} = 46.34$ and $\hat{\xi} = 0.114$.

Finally, Figure 8 shows a simulation of four consecutive days of rainfall from Model 1 with the estimated values of the parameters: $\delta = 0.577$, $\phi = 0.874$, $\psi_1 = 9.107$, $\psi_2 = 0.328$, $\sigma = 46.34$, $\xi = 0.114$. The simulated data below the 0.90 marginal quantile are censored and the value of the thresholds, which are spatially varying, are colored in blue and green. The areas colored in red and yellow are those with rainfall amounts exceeding the thresholds. Black points denote the stations observed in the data application. Since $\delta > 0.5$, the model is AD in space and AI in time: this results in a storm with extreme amounts of rainfall over the majority of the spatial domain at $t = 3$, but rapidly fading away in the following time period.

5. Conclusions

It is widely acknowledged in the literature that sub-asymptotic models should be employed to capture the dependence between values exceeding a convenient high threshold (Huser et al., 2025). However, the use of this type of models has mainly focused on spatial dependence, while spatio-temporal dependence is less studied. Indeed, the presence of a distinct type of extremal dependence in the spatial and temporal dimensions renders specification challenging. In comparison to previous attempts that have sought to achieve the same objective (Bortot and Gaetan, 2024), this work proposes a solution that has the advantage of being able to capture the different types of dependence through a parameter whose value can be estimated from the data. The estimation of this parameter, as well as the other model parameters, is achieved through the utilization of the computational power offered by modern numerical libraries for learning neural networks.

The proposed spatio-temporal model exhibits an extremal spatio-temporal dependence that is stationary within the specified period. In consideration of its potential application to

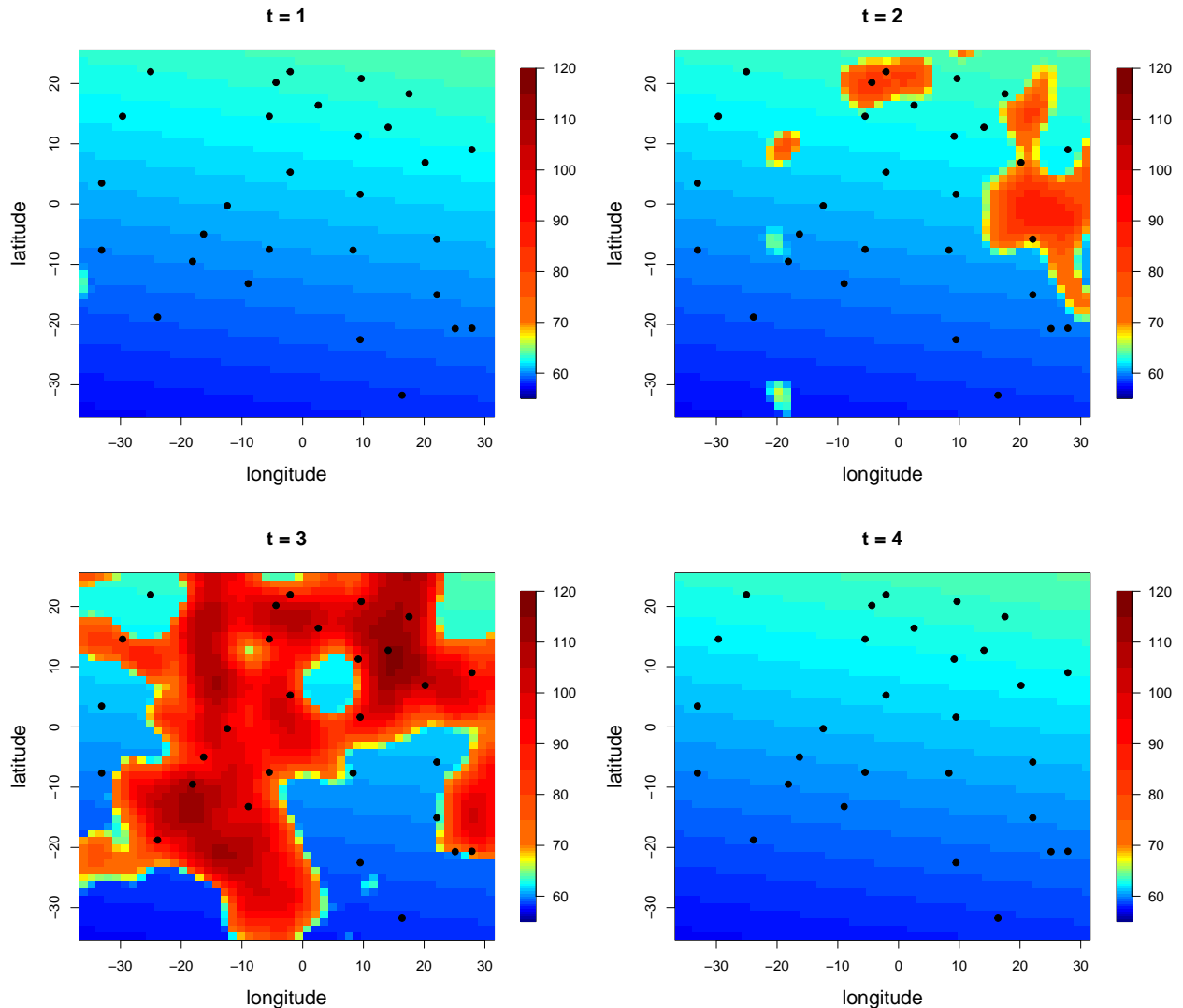


Figure 8: A simulation of four consecutive days of rainfall from Model 1 (see Table 1) with $\delta > 0.5$: AD in space and AI in time. Data exceeding the 0.90 marginal quantile are highlighted in red, while the rest of the data is censored and the estimated 0.90 quantiles are displayed. Black points denote the stations observed in the data application.

the study of climate change, a logical subsequent step is to consider a non-stationary model, similarly to the approach outlined in [Maume-Deschamps et al. \(2024\)](#). Moreover, in order to apply the model to larger spatial domains, the introduction of spatial non-stationarity would be an useful extension.

The flexibility of the models presented in this work makes them suitable for analyzing many type of data whose extremal dependence in space and time is of interest, and notably environmental data. Nevertheless, given the novelty of the employed parameter estimation method, a greater focus is needed on competitive model selection, which would require the

development of new diagnostic tools, and will be the subject of future research.

Acknowledgments

The authors thank Thomas Opitz for helpful discussions and suggestions about the random scale construction and Raphaël Huser for hints about the estimation method. The authors also thank the anonymous reviewers for their constructive suggestions that helped improve the quality of the manuscript.

References

- Ahmed, M., Maume-Deschamps, V., and Ribereau, P. (2022). Recognizing a spatial extreme dependence structure: A deep learning approach. Environmetrics, 33:e2714.
- Bacro, J.-N., Gaetan, C., Opitz, T., and Toulemonde, G. (2020). Hierarchical space-time modeling of exceedances with an application to rainfall data. Journal of the American Statistical Association, 115:555–569.
- Bacro, J. N., Gaetan, C., and Toulemonde, G. (2016). A flexible dependence model for spatial extremes. Journal of Statistical Planning and Inference, 172:36–52.
- Bortot, P., Coles, S., and Tawn, J. (2000). The multivariate Gaussian tail model: an application to oceanographic data. Journal of the Royal Statistical Society: Series C (Applied Statistics), 49:31–049.
- Bortot, P. and Gaetan, C. (2024). A model for space-time threshold exceedances with an application to extreme rainfall. Statistical Modelling, 24:169–193.
- Breiman, L. (1965). On some limit theorems similar to the arc-sin law. Theory of Probability & Its Applications, 10:323–331.
- Casson, E. and Coles, S. G. (1999). Spatial regression models for extremes. Extremes, 1:449–468.
- Castruccio, S., Huser, R., and Genton, M. (2016). High-order composite likelihood inference for max-stable distributions and processes. Journal of Computational and Graphical Statistics, 25:1212–1229.
- Chan, Y. and Li, H. (2008). Tail dependence for multivariate t-copulas and its monotonicity. Insurance: Mathematics and Economics, 42:763–770.
- Cooley, D., Nychka, D., and Naveau, P. (2007). Bayesian spatial modeling of extreme precipitation return levels. Journal of the American Statistical Association, 102:824–840.
- Davis, R. A. and Mikosch, T. (2008). Extreme value theory for space-time processes with heavy-tailed distributions. Stochastic Processes and their Applications, 118:560–584.

- Davison, A. C., Padoan, S. A., Ribatet, M., et al. (2012). Statistical modeling of spatial extremes. Statistical Science, 27:161–186.
- Davison, A. C. and Smith, R. L. (1990). Models for exceedances over high thresholds. Journal of the Royal Statistical Society: Series B (Statistical Methodology), 3:393–442.
- de Haan, L. (1984). A spectral representation for max-stable processes. The Annals of Probability, 12:1194–1204.
- Eastoe, E. F. and Tawn, J. A. (2009). Modelling non-stationary extremes with application to surface level ozone. Journal of the Royal Statistical Society: Series C (Applied Statistics), 58:25–45.
- Engelke, S., Opitz, T., and Wadsworth, J. L. (2019). Extremal dependence of random scale constructions. Extremes, 22:623–666.
- Fawcett, L. and Walshaw, D. (2006). Improved estimation for temporally clustered extremes. Environmetrics, 18:173–188.
- Gaetan, C. and Grigoletto, M. (2007). A hierarchical model for the analysis of spatial rainfall extremes. Journal of Agricultural, Biological, and Environmental Statistics, 12:434–449.
- Gerber, F. and Nychka, D. (2021). Fast covariance parameter estimation of spatial Gaussian process models using neural networks. Stat, 10:e382.
- Gneiting, T. (2002). Nonseparable, stationary covariance functions for space–time data. Journal of the American Statistical Association, 97:590–600.
- Huser, R. and Davison, A. C. (2014). Space-time modelling of extreme events. Journal of the Royal Statistical Society: Series B (Statistical Methodology), 76:439–461.
- Huser, R., Opitz, T., and Thibaud, E. (2017). Bridging asymptotic independence and dependence in spatial extremes using Gaussian scale mixtures. Spatial Statistics, 21:166–186.
- Huser, R., Opitz, T., and Wadsworth, J. L. (2025). Modeling of spatial extremes in environmental data science: time to move away from max-stable processes. Environmental Data Science, 4:e3.
- Huser, R. and Wadsworth, J. L. (2019). Modeling spatial processes with unknown extremal dependence class. Journal of the American Statistical Association, 114:434–444.
- Huser, R. and Wadsworth, J. L. (2020). Advances in statistical modeling of spatial extremes. Wiley Interdisciplinary Reviews: Computational Statistics, page e1537.
- Joe, H. (1997). Multivariate Models and Multivariate Dependence Concepts. Chapman and Hall/CRC.

- Johnson, N. L., Kotz, S., and Balakrishnan, N. (1994). Continuous Univariate Distributions, Volume 1. John Wiley & Sons, New York.
- Kalinowski, T., Allaire, J., and Chollet, F. (2024). keras3: R Interface to 'Keras'. R package version 1.2.0, <https://github.com/rstudio/keras3>.
- Kasahara, Y. (2018). A note on the product of independent random variables with regularly varying tails. Tsukuba Journal of Mathematics, 42:295–308.
- Kifer, Y. and Varadhan, S. (2017). Tails of polynomials of random variables and stable limits for nonconventional sums. Journal of Statistical Physics, 166:575–608.
- LeCun, Y., Bengio, Y., and Hinton, G. (2015). Deep learning. Nature, 521:436–444.
- Ledford, A. W. and Tawn, J. A. (1996). Statistics for near independence in multivariate extreme values. Biometrika, 83:169–187.
- Lenzi, A., Bessac, J., Rudi, J., and Stein, M. L. (2023). Neural networks for parameter estimation in intractable models. Computational Statistics & Data Analysis, 185:107762.
- Lopez Pinaya, W. H., Vieira, S., Garcia-Dias, R., and Mechelli, A. (2020). Chapter 10 - convolutional neural networks. In Mechelli, A. and Vieira, S., editors, Machine Learning, pages 173–191. Academic Press.
- Majumder, R. and Reich, B. J. (2023). A deep learning synthetic likelihood approximation of a non-stationary spatial model for extreme streamflow forecasting. Spatial Statistics, 55:100755.
- Majumder, R., Reich, B. J., and Shaby, B. A. (2024). Modeling extremal streamflow using deep learning approximations and a flexible spatial process. The Annals of Applied Statistics, 18:1519–1542.
- Maume-Deschamps, V., Ribereau, P., and Zeidan, M. (2024). A spatio-temporal model for temporal evolution of spatial extremal dependence. Spatial Statistics, 64:100860.
- Morris, S. A., Reich, B. J., Thibaud, E., and Cooley, D. (2017). A space-time skew-t model for threshold exceedances. Biometrics, 73:749–758.
- Padoan, S. A., Ribatet, M., and Sisson, S. A. (2010). Likelihood-based inference for max-stable processes. Journal of the American Statistical Association, 105:263–277.
- Richards, J., Sainsbury-Dale, M., Zammit-Mangion, A., and Huser, R. (2024). Neural Bayes estimators for censored inference with peaks-over-threshold models. Journal of Machine Learning Research, 25:1–49.
- Røislien, J. and Omre, H. (2006). T-distributed random fields: a parametric model for heavy-tailed well-log data. Mathematical Geology, 38:821–849.

- Sainsbury-Dale, M., Zammit-Mangion, A., and Huser, R. (2024). Likelihood-free parameter estimation with neural Bayes estimators. The American Statistician, 78:1–14.
- Sang, H. and Gelfand, A. (2009). Hierarchical modeling for extreme values observed over space and time. Environmental and Ecological Statistics, 16:407–426.
- Sang, H. and Gelfand, A. E. (2010). Continuous spatial process models for spatial extreme values. Journal of Agricultural, Biological, and Environmental Statistics, 15:49–65.
- Schlather, M. (2002). Models for stationary max-stable random fields. Extremes, 5:33–44.
- Sibuya, M. (1960). Bivariate extreme statistics, I. Annals of the Institute of Statistical Mathematics, 11:195–210.
- Simpson, E. S., Opitz, T., and Wadsworth, J. L. (2023). High-dimensional modeling of spatial and spatio-temporal conditional extremes using INLA and Gaussian Markov random fields. Extremes, 26:669–713.
- Simpson, E. S. and Wadsworth, J. L. (2021). Conditional modelling of spatio-temporal extremes for Red Sea surface temperatures. Spatial Statistics, 41:100482.
- Smith, R. L. (1990). Max-stable processes and spatial extremes. Preprint. University of Surrey.
- Steinkohl, C., Davis, R., and Klüppelberg, C. (2013). Extreme value analysis of multivariate high-frequency wind speed data. Journal of Statistical Theory and Practice, 7:73–94.
- Tawn, J., Shooter, R., Towe, R., and Lamb, R. (2018). Modelling spatial extreme events with environmental applications. Spatial Statistics, 28:39–58.
- Varin, C., Reid, N., and Firth, D. (2011). An overview of composite likelihood methods. Statistica Sinica, 21:5–42.
- Wadsworth, J. and Tawn, J. (2022). Higher-dimensional spatial extremes via single-site conditioning. Spatial Statistics, 51:100677.
- Wadsworth, J. and Tawn, J. A. (2012). Dependence modelling for spatial extremes. Biometrika, 99:253–272.
- Wixson, T. P. and Cooley, D. (2024). Neural network for asymptotic dependence/independence classification: A series of experiments.
- Zhang, L., Shaby, B. A., and Wadsworth, J. L. (2022). Hierarchical transformed scale mixtures for flexible modeling of spatial extremes on datasets with many locations. Journal of the American Statistical Association, 117:1357–1369.

Appendix A. Proof on dependence properties (pairs in time and space-time)

This appendix contains the proofs on the dependence properties of model (4) stated in Section 2.3, for pairs in time and space-time. Pairs in space are covered by Appendix B. Let $(X_1, X_2) = (R_1^\delta W_1^{1-\delta}, R_2^\delta W_2^{1-\delta})$, with $X_i := X(s_i, t_i)$, $R_i := R(t_i)$ and $W_i := W(s_i, t_i)$, for $i = 1, 2$, such that $t_1 \neq t_2$, be a generic pair from model (4). To study the extremal dependence of (X_1, X_2) , we have to compute their coefficient χ_X , equivalent to the one defined in (1), and in particular its numerator, for a fixed u , $\mathbb{P}(X_1 > F_{X_1}^{-1}(u), X_2 > F_{X_2}^{-1}(u))$.

Case 1: $\delta < 0.5$ (third column of Table 1)

(X_1, X_2) belong to the same extremal dependence class as (W_1, W_2) , i.e.,

- (X_1, X_2) are AI if (W_1, W_2) are AI, with $\eta_W < 1$;
- (X_1, X_2) are AD if (W_1, W_2) are AD.

Proof: By Breiman's lemma (Breiman, 1965, see also Engelke et al., 2019, Lemma 8), as $x \rightarrow \infty$,

$$\mathbb{P}(X_1 > x) = \bar{F}_{X_1}(x) \sim \mathbb{E}\left(R_1^{\delta/(1-\delta)}\right) \bar{F}_{W_1^{1-\delta}}(x) = \frac{1-\delta}{1-2\delta} x^{-1/(1-\delta)},$$

and, as $u \rightarrow 1$ (see Engelke et al., 2019, eq. 22),

$$F_{X_1}^{-1}(u) \sim \mathbb{E}\left(R_1^{\delta/(1-\delta)}\right)^{1-\delta} F_{W_1^{1-\delta}}^{-1}(u) = \left(\frac{1-\delta}{1-2\delta}\right)^{1-\delta} \left(\frac{1}{1-u}\right)^{1-\delta}.$$

Therefore, as $u \rightarrow 1$, the numerator of χ_X is

$$\begin{aligned} \mathbb{P}(X_1 > F_{X_1}^{-1}(u), X_2 > F_{X_2}^{-1}(u)) &\sim \mathbb{P}\left(X_1 > \left(\frac{1-\delta}{1-2\delta}\right)^{1-\delta} \left(\frac{1}{1-u}\right)^{1-\delta}, X_2 > \left(\frac{1-\delta}{1-2\delta}\right)^{1-\delta} \left(\frac{1}{1-u}\right)^{1-\delta}\right) \\ &= \mathbb{P}\left(R_1^{\delta/(1-\delta)} W_1 > \frac{1-\delta}{(1-2\delta)(1-u)}, R_2^{\delta/(1-\delta)} W_2 > \frac{1-\delta}{(1-2\delta)(1-u)}\right) \\ &< \mathbb{P}\left(R_1^{\delta/(1-\delta)} W_1 > \frac{1}{1-u}, R_2^{\delta/(1-\delta)} W_2 > \frac{1}{1-u}\right) \\ &= \mathbb{P}\left(\min\left\{R_1^{\delta/(1-\delta)} W_1, R_2^{\delta/(1-\delta)} W_2\right\} > \frac{1}{1-u}\right) \\ &< \mathbb{P}\left(R_1^{\delta/(1-\delta)} \min\{W_1, W_2\} > \frac{1}{1-u}\right) + \\ &\quad + \mathbb{P}\left(R_2^{\delta/(1-\delta)} \min\{W_1, W_2\} > \frac{1}{1-u}\right) \\ &\sim 2 \cdot (1-u)^{\min\{(1-\delta)/\delta, 1/\eta_W\}}, \end{aligned}$$

where the last line derives from Breiman's Lemma, noting that, as $u \rightarrow 1$, $\bar{F}_{\min\{W_1, W_2\}}(x) \sim x^{-1/\eta_W}$, while $\bar{F}_{R_i^{\delta/(1-\delta)}}(x) \sim x^{-(1-\delta)/\delta}$, for $i = 1, 2$. Then, if (W_1, W_2) are AI with $\eta_W < 1$, $\min\{(1-\delta)/\delta, 1/\eta_W\} > 1$ and

$$\chi_X = \lim_{u \rightarrow 1} \frac{\mathbb{P}(X_1 > F_{X_1}^{-1}(u), X_2 > F_{X_2}^{-1}(u))}{1-u} \leq \lim_{u \rightarrow 1} \frac{(1-u)^{\min\{\frac{1-\delta}{\delta}, \frac{1}{\eta_W}\}}}{1-u} = 0,$$

i.e. (X_1, X_2) are AI, with $\eta_X \leq \max\{\delta/(1-\delta), \eta_W\} < 1$.

On the other hand,

$$\begin{aligned} \mathbb{P}(X_1 > F_{X_1}^{-1}(u), X_2 > F_{X_2}^{-1}(u)) &\sim \mathbb{P}\left(X_1 > \left(\frac{1-\delta}{1-2\delta}\right)^{1-\delta} \left(\frac{1}{1-u}\right)^{1-\delta}, X_2 > \left(\frac{1-\delta}{1-2\delta}\right)^{1-\delta} \left(\frac{1}{1-u}\right)^{1-\delta}\right) \\ &= \mathbb{P}\left(R_1^{\delta/(1-\delta)} W_1 > \frac{1-\delta}{(1-2\delta)(1-u)}, R_2^{\delta/(1-\delta)} W_2 > \frac{1-\delta}{(1-2\delta)(1-u)}\right) \\ &= \mathbb{P}\left(\min\left\{R_1^{\delta/(1-\delta)} W_1, R_2^{\delta/(1-\delta)} W_2\right\} > \frac{1-\delta}{(1-2\delta)(1-u)}\right) \\ &\geq \mathbb{P}\left(\min\{R_1, R_2\}^{\delta/(1-\delta)} \min\{W_1, W_2\} > \frac{1-\delta}{(1-2\delta)(1-u)}\right) \\ &\sim c(\delta) (1-u)^{\min\{(1-\delta)/(\delta \cdot \eta_R), 1/\eta_W\}}, \end{aligned}$$

with $c(\delta) > 0$ for all $\delta < 0.5$. If (W_1, W_2) are AD, $\eta_W = 1$, so $\min\{(1-\delta)/(\delta \cdot \eta_R), 1/\eta_W\} = 1$ and

$$\chi_X = \lim_{u \rightarrow 1} \frac{\mathbb{P}(X_1 > F_{X_1}^{-1}(u), X_2 > F_{X_2}^{-1}(u))}{1-u} \geq \lim_{u \rightarrow 1} \frac{c(\delta)(1-u)}{1-u} > 0,$$

i.e. (X_1, X_2) are AD.

Case 2: $\delta > 0.5$ (first column of Table 1)

(X_1, X_2) belong to the same extremal dependence class as (R_1, R_2) , i.e.,

- (X_1, X_2) are AI if (R_1, R_2) are AI, with $\eta_W < 1$;
- (X_1, X_2) are AD if (R_1, R_2) are AD.

Proof: By Breiman's lemma,

$$\mathbb{P}(X_1 > x) = \bar{F}_{X_1}(x) \sim \mathbb{E}\left(W_1^{(1-\delta)/\delta}\right) \bar{F}_{R_1^\delta}(x) = \frac{\delta}{2\delta-1} x^{-1/\delta},$$

$$F_{X_1}^{-1}(u) \sim \mathbb{E}\left(W_1^{(1-\delta)/\delta}\right)^\delta F_{R_1^\delta}^{-1}(u) = \left(\frac{\delta}{2\delta-1}\right)^\delta \left(\frac{1}{1-u}\right)^\delta.$$

Therefore, similarly to Case 1, as $u \rightarrow 1$ the numerator of χ_X is

$$\begin{aligned}
\mathbb{P}(X_1 > F_{X_1}^{-1}(u), X_2 > F_{X_2}^{-1}(u)) &\sim \mathbb{P}\left(X_1 > \left(\frac{\delta}{2\delta-1}\right)^\delta \left(\frac{1}{1-u}\right)^\delta, X_2 > \left(\frac{\delta}{2\delta-1}\right)^\delta \left(\frac{1}{1-u}\right)^\delta\right) \\
&< \mathbb{P}\left(R_1 W_1^{(1-\delta)/\delta} > \frac{1}{1-u}, R_2 W_2^{(1-\delta)/\delta} > \frac{1}{1-u}\right) \\
&< \mathbb{P}\left(\min\{R_1, R_2\} W_1^{(1-\delta)/\delta} > \frac{1}{1-u}\right) + \\
&\quad + \mathbb{P}\left(\min\{R_1, R_2\} W_2^{(1-\delta)/\delta} > \frac{1}{1-u}\right) \\
&\sim 2 \cdot (1-u)^{\min\{(\delta/(1-\delta), 1/\eta_R)\}},
\end{aligned}$$

where the last line derives from Breiman's Lemma, noting that, as $u \rightarrow 1$, $\bar{F}_{\min\{R_1, R_2\}}(x) \sim x^{-1/\eta_R}$, while $\bar{F}_{W_i^{(1-\delta)/\delta}}(x) \sim x^{-\delta/(1-\delta)}$, for $i = 1, 2$. Then, if (R_1, R_2) are AI with $\eta_R < 1$, $\min\{(\delta/(1-\delta), 1/\eta_R)\} > 1$ and

$$\chi_X = \lim_{u \rightarrow 1} \frac{\mathbb{P}(X_1 > F_{X_1}^{-1}(u), X_2 > F_{X_2}^{-1}(u))}{1-u} \leq \lim_{u \rightarrow 1} \frac{(1-u)^{\min\{(\delta/(1-\delta), 1/\eta_R)\}}}{1-u} = 0,$$

i.e. (X_1, X_2) are AI, with $\eta_X \leq \max\{(1-\delta)/\delta, \eta_R\} < 1$.

On the other hand, similarly to Case 1,

$$\begin{aligned}
\mathbb{P}(X_1 > F_{X_1}^{-1}(u), X_2 > F_{X_2}^{-1}(u)) &\sim \mathbb{P}\left(X_1 > \left(\frac{\delta}{2\delta-1}\right)^\delta \left(\frac{1}{1-u}\right)^\delta, X_2 > \left(\frac{\delta}{2\delta-1}\right)^\delta \left(\frac{1}{1-u}\right)^\delta\right) \\
&\geq \mathbb{P}\left(\min\{R_1, R_2\} \min\{W_1, W_2\}^{(1-\delta)/\delta} > \frac{\delta}{(2\delta-1)(1-u)}\right) \\
&\sim c(\delta) (1-u)^{\min\{1/\eta_R, \delta/[(1-\delta)\eta_W]\}},
\end{aligned}$$

with $c(\delta) > 0$ for all $\delta > 0.5$. If (R_1, R_2) are AD, then $\eta_R = 1$, so $\min\{1/\eta_R, \delta/[(1-\delta)\eta_W]\} = 1$ and

$$\chi_X = \lim_{u \rightarrow 1} \frac{\mathbb{P}(X_1 > F_{X_1}^{-1}(u), X_2 > F_{X_2}^{-1}(u))}{1-u} \geq \lim_{u \rightarrow 1} \frac{c(\delta)(1-u)}{1-u} > 0,$$

i.e. (X_1, X_2) are AD.

Case 3: $\delta = 0.5$ (second column of Table 1)

(X_1, X_2) are AI, unless both (W_1, W_2) and (R_1, R_2) are AD, i.e.

- (X_1, X_2) are AI, with $\eta_X < 1$ if $(W_1, W_2), (R_1, R_2)$ are AI, with $\eta_W < 1, \eta_R < 1$;
- (X_1, X_2) are AI, with $\eta_X = 1$ if (W_1, W_2) are AI, with $\eta_W < 1$, and (R_1, R_2) are AD;
- (X_1, X_2) are AI, with $\eta_X = 1$ if (W_1, W_2) are AD and (R_1, R_2) are AI, with $\eta_R < 1$;
- (X_1, X_2) are AD if (W_1, W_2) are AD and (R_1, R_2) are AD.

Proof: Since $X_1 = R_1^{1/2}W_1^{1/2}$ and $X_2 = R_2^{1/2}W_2^{1/2}$ have the same marginal distribution, we can compute χ_X in (1) as

$$\chi_X = \lim_{x \rightarrow \infty} \frac{\mathbb{P}(X_1 > x, X_2 > x)}{\mathbb{P}(X_1 > x)}.$$

Note that, as reported in (5), the denominator is equal to

$$\mathbb{P}(X_1 > x) = x^{-2} [2 \log(x) + 1].$$

If (W_1, W_2) are AI with $\eta_W < 1$ and (R_1, R_2) are AD, the numerator is such that

$$\begin{aligned} \mathbb{P}(X_1 > x, X_2 > x) &= \mathbb{P}\left(R_1^{1/2}W_1^{1/2} > x, R_2^{1/2}W_2^{1/2} > x\right) = \mathbb{P}\left(\min\{R_1W_1, R_2W_2\} > x^2\right) \\ &\leq \mathbb{P}\left(R_1 \min\{W_1, W_2\} > x^2 \cap R_1 > R_2\right) + \\ &\quad + \mathbb{P}\left(R_2 \min\{W_1, W_2\} > x^2 \cap R_1 \leq R_2\right) \\ &\leq \mathbb{P}\left(R_1 \min\{W_1, W_2\} > x^2\right) + \mathbb{P}\left(R_2 \min\{W_1, W_2\} > x^2\right) \\ &\sim 2 \mathbb{E}[\min\{W_1, W_2\}] \bar{F}_R(x^2) = 2 \mathbb{E}[\min\{W_1, W_2\}] x^{-2}. \end{aligned}$$

Therefore,

$$\chi_X = \lim_{x \rightarrow \infty} \frac{\mathbb{P}(X_1 > x, X_2 > x)}{\mathbb{P}(X_1 > x)} \leq \lim_{x \rightarrow \infty} \frac{2 \mathbb{E}[\min\{W_1, W_2\}] x^{-2}}{x^{-2} [2 \log(x) + 1]} = 0,$$

i.e. (X_1, X_2) are AI, although $\eta_X = 1$.

If (R_1, R_2) are AI with $\eta_R < 1$ and (W_1, W_2) are AD, the numerator is such that

$$\begin{aligned} \mathbb{P}(X_1 > x, X_2 > x) &= \mathbb{P}\left(R_1^{1/2}W_1^{1/2} > x, R_2^{1/2}W_2^{1/2} > x\right) = \mathbb{P}\left(\min\{R_1W_1, R_2W_2\} > x^2\right) \\ &\leq \mathbb{P}\left(W_1 \min\{R_1, R_2\} > x^2\right) + \mathbb{P}\left(W_2 \min\{R_1, R_2\} > x^2\right) \\ &\sim 2 \mathbb{E}[\min\{R_1, R_2\}] \bar{F}_W(x^2) = 2 \mathbb{E}[\min\{R_1, R_2\}] x^{-2}. \end{aligned}$$

Therefore,

$$\chi_X = \lim_{x \rightarrow \infty} \frac{\mathbb{P}(X_1 > x, X_2 > x)}{\mathbb{P}(X_1 > x)} \leq \lim_{x \rightarrow \infty} \frac{2 \mathbb{E}[\min\{R_1, R_2\}] x^{-2}}{x^{-2} [2 \log(x) + 1]} = 0,$$

i.e. (X_1, X_2) are AI, although $\eta_X = 1$.

If (W_1, W_2) are AI with $\eta_W < 1$ and (R_1, R_2) are AI with $\eta_R < 1$, the numerator is

$$\mathbb{P}(X_1 > x, X_2 > x) \sim c x^{-2 \min\{1/\eta_W, 1/\eta_R\}},$$

so $\chi_X = 0$ and (X_1, X_2) are AI with $\eta_X = \max\{\eta_W, \eta_R\} < 1$.

If both (W_1, W_2) and (R_1, R_2) are AD, the numerator is such that

$$\begin{aligned} \mathbb{P}(X_1 > x, X_2 > x) &= \mathbb{P}\left(\min\left\{R_1^{1/2}W_1^{1/2}, R_2^{1/2}W_2^{1/2}\right\} > x\right) \\ &\geq \mathbb{P}\left(\min\{R_1, R_2\}^{1/2} \min\{W_1, W_2\}^{1/2} > x\right). \end{aligned}$$

We use the result (1.5) from [Kasahara \(2018\)](#), proved by [Kifer and Varadhan \(2017\)](#): if Z_1, Z_2 are independent random variables such that

$$\mathbb{P}(Z_j > z) \sim c_j z^{-\alpha_j} (\log z)^{k_j}, \quad j = 1, 2,$$

and $\alpha_1 = \alpha_2$, then

$$\mathbb{P}(Z_1 Z_2 > z) \sim \alpha_1 B(k_1 + 1, k_2 + 1) c_1 c_2 z^{-\alpha_1} (\log z)^{k_1 + k_2 + 1}.$$

Note that

$$\mathbb{P}(\min\{R_1, R_2\}^{1/2} > x) \sim L_R(x^2) x^{-2} \quad \text{and} \quad \mathbb{P}(\min\{W_1, W_2\}^{1/2} > x) \sim L_W(x^2) x^{-2},$$

$$\text{with } L_R(x^2) \rightarrow \chi_R > 0 \quad \text{and} \quad L_W(x^2) \rightarrow \chi_W > 0, \text{ as } x \rightarrow \infty,$$

i.e. there exist a positive constant $\varepsilon < \min\{\chi_R, \chi_W\}$ and x_ε such that, for all $x > x_\varepsilon$,

$$L_R(x^2) \geq \chi_R - \varepsilon \quad \text{and} \quad L_W(x^2) \geq \chi_W - \varepsilon.$$

Then, for large x ,

$$\mathbb{P}(\min\{R_1, R_2\}^{1/2} \min\{W_1, W_2\}^{1/2} > x) \geq c x^{-2} \log x,$$

with $c = (\chi_R - \varepsilon)(\chi_W - \varepsilon)$, and

$$\chi_X = \lim_{x \rightarrow \infty} \frac{\mathbb{P}(X_1 > x, X_2 > x)}{\mathbb{P}(X_1 > x)} \geq c > 0,$$

i.e. (X_1, X_2) are AD.

Appendix B. Proof on dependence properties (pairs in space)

This appendix contains the proofs regarding the dependence properties of model (4) that are stated in Section 2.3 for pairs of observations in different locations and contemporaneous times. Let $(X_1, X_2) = (R_1^\delta W_1^{1-\delta}, R_2^\delta W_2^{1-\delta})$, with $X_i := X(s_i, t_i)$, $R_i := R(t_i)$ and $W_i := W(s_i, t_i)$, for $i = 1, 2$, such that $s_1 \neq s_2$ and $t_1 = t_2$, be a generic spatial pair from model (4). Since $R_1 = R_2$, we refer to them as R in the following. These proofs are based on some modifications of those in [Appendix A](#).

Case 1: $\delta < 0.5$ (third column of Table 1)

(X_1, X_2) belong to the same extremal dependence class as (W_1, W_2) , i.e.,

- (X_1, X_2) are AI if (W_1, W_2) are AI, with $\eta_W < 1$;
- (X_1, X_2) are AD if (W_1, W_2) are AD.

Proof: Similarly to Case 1 in [Appendix A](#), as $u \rightarrow 1$, the numerator of χ_X is

$$\begin{aligned} \mathbb{P}(X_1 > F_{X_1}^{-1}(u), X_2 > F_{X_2}^{-1}(u)) &< \mathbb{P}\left(\min\{R^{\delta/(1-\delta)}W_1, R^{\delta/(1-\delta)}W_2\} > \frac{1}{1-u}\right) \\ &= \mathbb{P}\left(R^{\delta/(1-\delta)}\min\{W_1, W_2\} > \frac{1}{1-u}\right) \\ &\sim (1-u)^{\min\{(1-\delta)/\delta, 1/\eta_W\}}. \end{aligned}$$

The last line derives from Breiman's Lemma, since, as $u \rightarrow 1$, $\bar{F}_{\min\{W_1, W_2\}}(x) \sim x^{-1/\eta_W}$, and $\bar{F}_{R^{\delta/(1-\delta)}}(x) \sim x^{-(1-\delta)/\delta}$.

If (W_1, W_2) are AI with $\eta_W < 1$, $\min\{(1-\delta)/\delta, 1/\eta_W\} > 1$ and

$$\chi_X = \lim_{u \rightarrow 1} \frac{\mathbb{P}(X_1 > F_{X_1}^{-1}(u), X_2 > F_{X_2}^{-1}(u))}{1-u} \leq \lim_{u \rightarrow 1} \frac{(1-u)^{\min\{(1-\delta)/\delta, 1/\eta_W\}}}{1-u} = 0,$$

i.e. (X_1, X_2) are AI, with $\eta_X \leq \max\{\delta/(1-\delta), \eta_W\} < 1$.

On the other hand,

$$\begin{aligned} \mathbb{P}(X_1 > F_{X_1}^{-1}(u), X_2 > F_{X_2}^{-1}(u)) &\sim \mathbb{P}\left(R^{\delta/(1-\delta)}\min\{W_1, W_2\} > \frac{1-\delta}{(1-2\delta)(1-u)}\right) \\ &\sim c(\delta)(1-u)^{\min\{(1-\delta)/\delta, 1/\eta_W\}}, \end{aligned}$$

with $c(\delta) > 0$ for all $\delta < 0.5$.

If (W_1, W_2) are AD, then $\eta_W = 1$, so $\min\{(1-\delta)/\delta, 1/\eta_W\} = 1$ and

$$\chi_X = \lim_{u \rightarrow 1} \frac{\mathbb{P}(X_1 > F_{X_1}^{-1}(u), X_2 > F_{X_2}^{-1}(u))}{1-u} \geq \lim_{u \rightarrow 1} \frac{c(\delta)(1-u)}{1-u} > 0,$$

i.e. (X_1, X_2) are AD.

Case 2: $\delta > 0.5$ (first column of Table 1)

(X_1, X_2) are AD.

Proof: Similarly to Case 2 in Appendix A, as $u \rightarrow 1$, the numerator of χ_X is

$$\begin{aligned} \mathbb{P}(X_1 > F_{X_1}^{-1}(u), X_2 > F_{X_2}^{-1}(u)) &\geq \mathbb{P}\left(R \min\{W_1, W_2\}^{(1-\delta)/\delta} > \frac{\delta}{(2\delta-1)(1-u)}\right) \\ &\sim c(\delta) (1-u)^{\min\{1, \delta/[(1-\delta)\cdot\eta_W]\}} \end{aligned}$$

with $c(\delta) > 0$ for all $\delta > 0.5$. Since $\min\{1, \delta/[(1-\delta)\cdot\eta_W]\} = 1$,

$$\chi_X = \lim_{u \rightarrow 1} \frac{\mathbb{P}(X_1 > F_{X_1}^{-1}(u), X_2 > F_{X_2}^{-1}(u))}{1-u} \geq \lim_{u \rightarrow 1} \frac{c(\delta)(1-u)}{1-u} > 0,$$

i.e. (X_1, X_2) are AD.

Case 3: $\delta = 0.5$ (second column of Table 1)

(X_1, X_2) belong to the same extremal dependence class as (W_1, W_2) , i.e.,

- (X_1, X_2) are AI, with $\eta_X = 1$ if (W_1, W_2) are AI, with $\eta_W < 1$;
- (X_1, X_2) are AD if (W_1, W_2) are AD.

Proof: As in Case 3 of Appendix A, the denominator of χ_X is equal to

$$\mathbb{P}(X_1 > x) = x^{-2} [2 \log(x) + 1].$$

If (W_1, W_2) are AI with $\eta_W < 1$, the numerator is such that

$$\begin{aligned} \mathbb{P}(X_1 > x, X_2 > x) &= \mathbb{P}\left(R^{1/2} W_1^{1/2} > x, R^{1/2} W_2^{1/2} > x\right) = \mathbb{P}\left(R \min\{W_1, W_2\} > x^2\right) \\ &\sim \mathbb{E}[\min\{W_1, W_2\}] \bar{F}_R(x^2) = \mathbb{E}[\min\{W_1, W_2\}] x^{-2}. \end{aligned}$$

Therefore,

$$\chi_X = \lim_{x \rightarrow \infty} \frac{\mathbb{P}(X_1 > x, X_2 > x)}{\mathbb{P}(X_1 > x)} = \lim_{x \rightarrow \infty} \frac{\mathbb{E}[\min\{W_1, W_2\}] x^{-2}}{x^{-2} [2 \log(x) + 1]} = 0,$$

i.e. (X_1, X_2) are AI, although $\eta_X = 1$.

If (W_1, W_2) are AD, the numerator is such that

$$\begin{aligned} \mathbb{P}(X_1 > x, X_2 > x) &= \mathbb{P}\left(R^{1/2} \min\{W_1^{1/2}, W_2^{1/2}\} > x\right) \\ &\geq c x^{-2} \log x, \end{aligned}$$

with $c = \chi_W - \varepsilon$, for small $\varepsilon > 0$. The last inequality is derived using the same results as in the last point of Case 3 in Appendix A, since $\mathbb{P}(R^{1/2} > x) = x^{-2}$. Then,

$$\chi_X = \lim_{x \rightarrow \infty} \frac{\mathbb{P}(X_1 > x, X_2 > x)}{\mathbb{P}(X_1 > x)} \geq c > 0,$$

i.e. (X_1, X_2) are AD.

Supplementary material

S1. Simulation study

Figure S1 shows the estimated values for δ in $\{0.1, 0.2, \dots, 0.9\}$ for Model 2 and Model 4, to be compared with Figure 3 in the main text (Model 1 and Model 3). Among the four models, the one on which the estimation seems to have the worst performance is Model 4, in which all the components of the mixture are AD and δ does not discriminate between extremal dependence classes (see Table 1 in the main text).

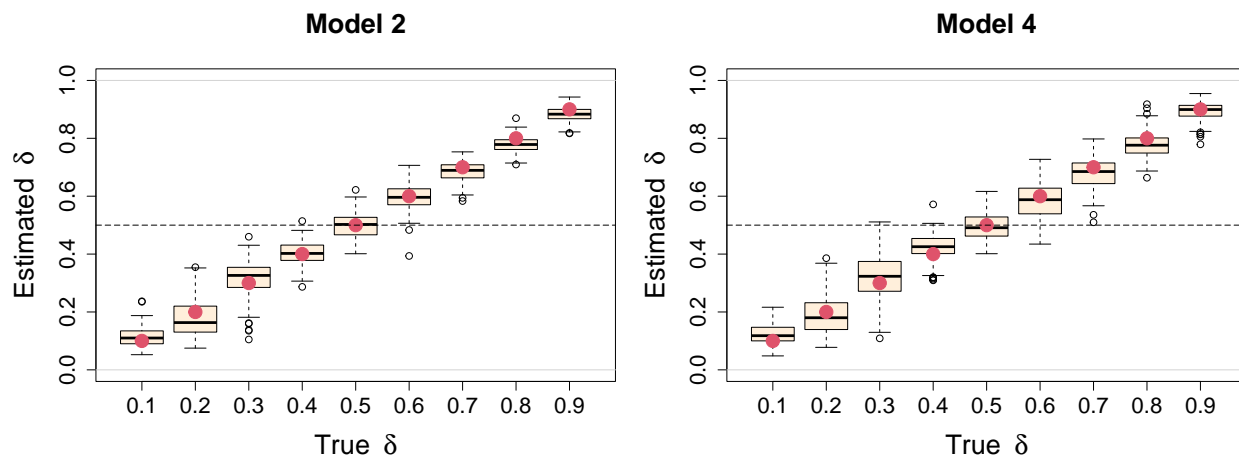


Figure S1: True (red points) and estimated (boxplots) values of δ on 200 independently simulated datasets, for Model 2 (left) and Model 4 (right).

Figure S2 shows the boxplots relative to the simulation study on ψ_1 , ψ_2 and ϕ for Model 2 and Model 4, to be compared with Figure 4 in the main text (Model 1 and Model 3).

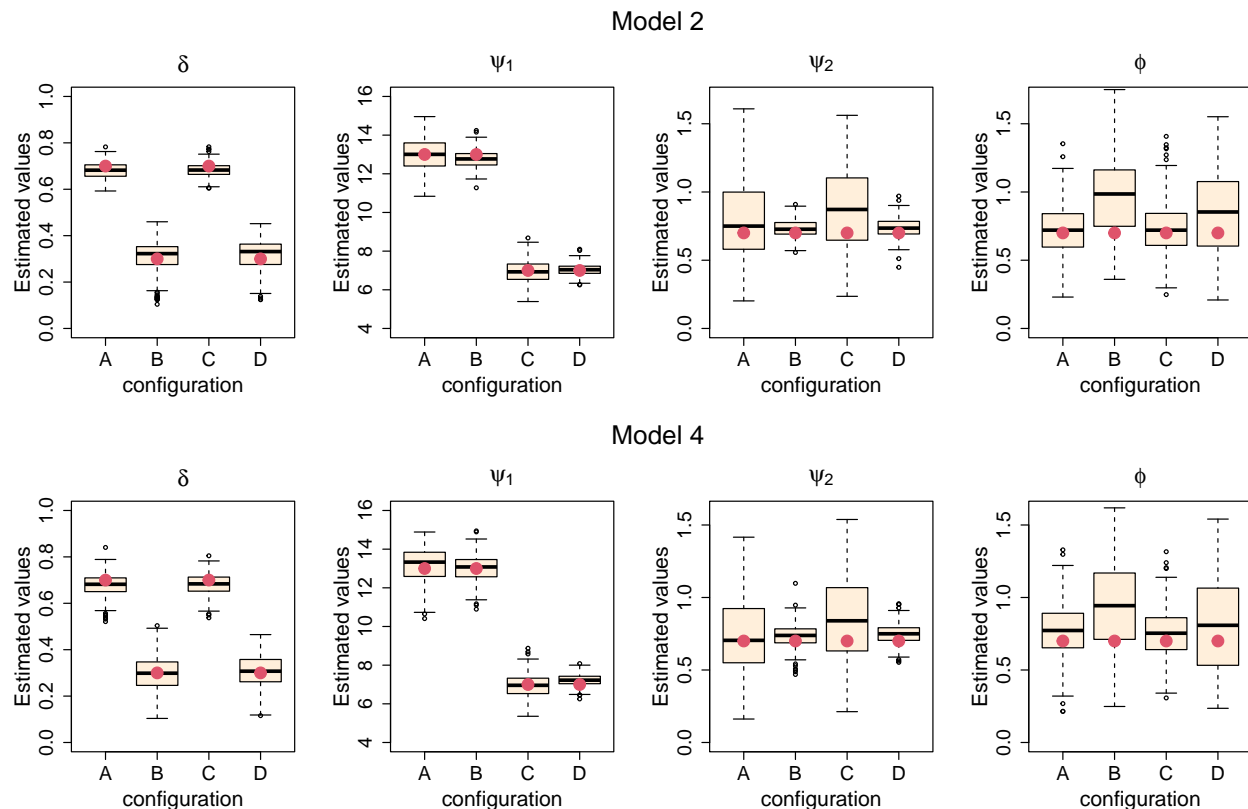


Figure S2: Boxplots of estimated values for $\delta = 0.7$ (A,C) or $\delta = 0.3$ (B,D), $\psi_1 = 13$ (A,B) or $\psi_1 = 7$ (C,D), $\psi_2 = 0.7$ and $\phi = 0.7$ (red points) on 400 simulated datasets from Model 2 and Model 4.

S2. Results and diagnostics

This section presents some results about the real data application with a correlation function different from that presented in section 4.2. In particular, the correlation function of the Gaussian process on which $W(s, t)$ is built is here $\rho_{W^*}(h, k; \psi) = [1 + (\|h\|/\psi_1)^2]^{-1} \times \exp\{-(k/\psi_2)^2\}$, for spatial lag h and temporal lag k .

Figure S3 shows the empirical pairwise coefficient $\hat{\chi}_{1,2}(u)$, for pairs (Y_1, Y_2) at different distances in space and time and for $u \in \{0.9, 0.95, 0.99\}$. Compared with Figure 6 in the main text, it does not present substantial differences.

Table S1 displays the $\text{RMSE}(k, u)$ for Model 1 and Model 3, to be compared with those of Table 3 in the main text. The values indicate a slight preference for the correlation function presented in the text, compared to the one presented here.

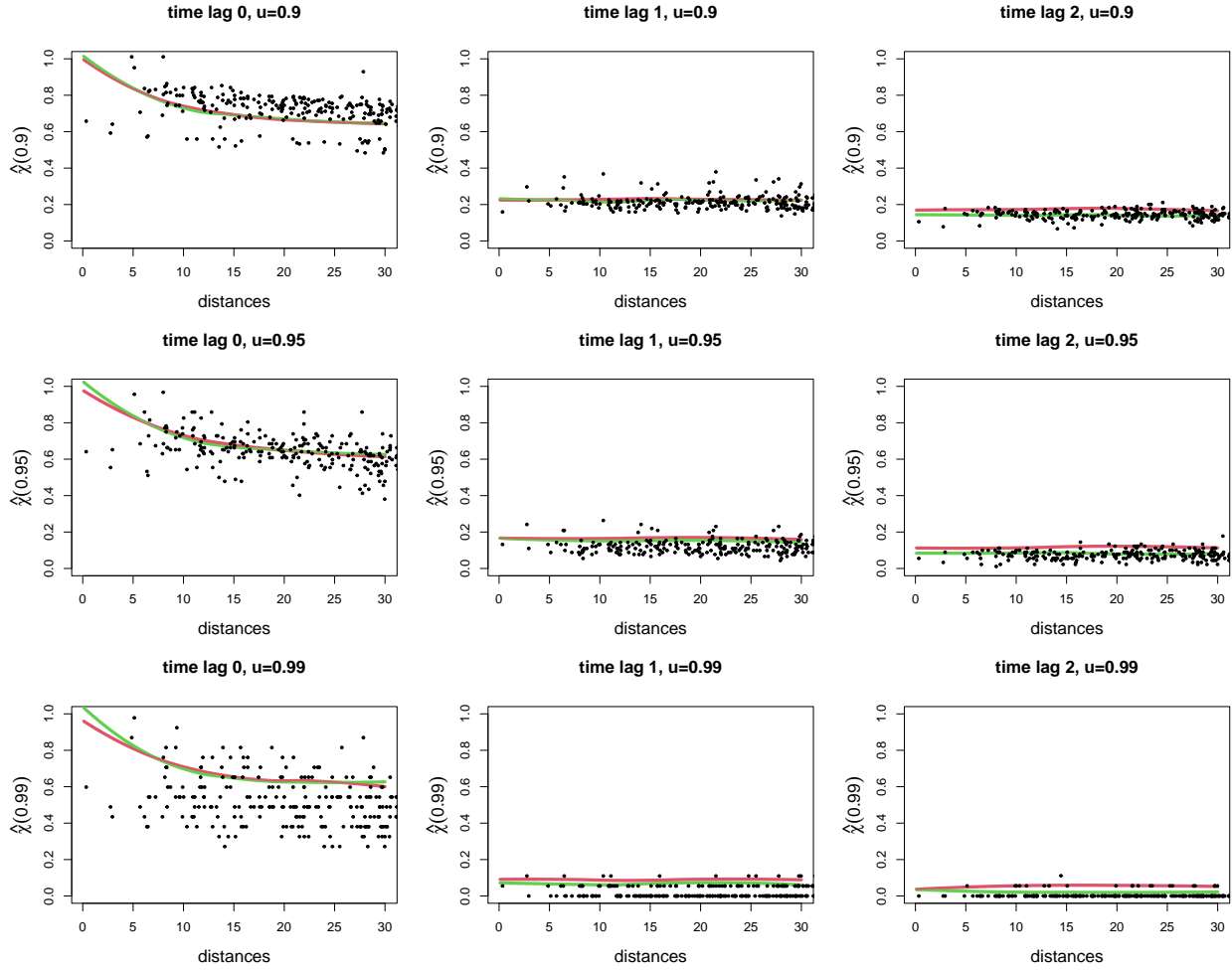


Figure S3: Values of $\chi(u)$ for different spatial distances and temporal lags, derived from the estimated Model 1 (red lines), from the Model 3 (green lines) and the empirical ones for each pair of stations (dots).

Model	$k = 0$		$k = 1$		$k = 2$	
	$u = 0.9$	$u = 0.95$	$u = 0.9$	$u = 0.95$	$u = 0.9$	$u = 0.95$
1	0.115	0.145	0.026	0.028	0.027	0.029
3	0.108	0.113	0.029	0.031	0.028	0.030

Table S1: $\text{RMSE}(k, u)$ between empirical estimates of $\chi_{s_i; k}^*(u)$ and estimates from Model 1 and Model 3.

S3. Marginal parameter estimation

Figure S4 shows site-specific estimates and 95% confidence intervals for the marginal parameter σ and ξ . The horizontal lines represent the estimates of the two parameters obtained by fitting the GPD model on all the threshold exceedances together. The horizontal lines intersect all of the site-wise confidence intervals, supporting the hypothesis of constant σ and ξ for the North Brabant data.

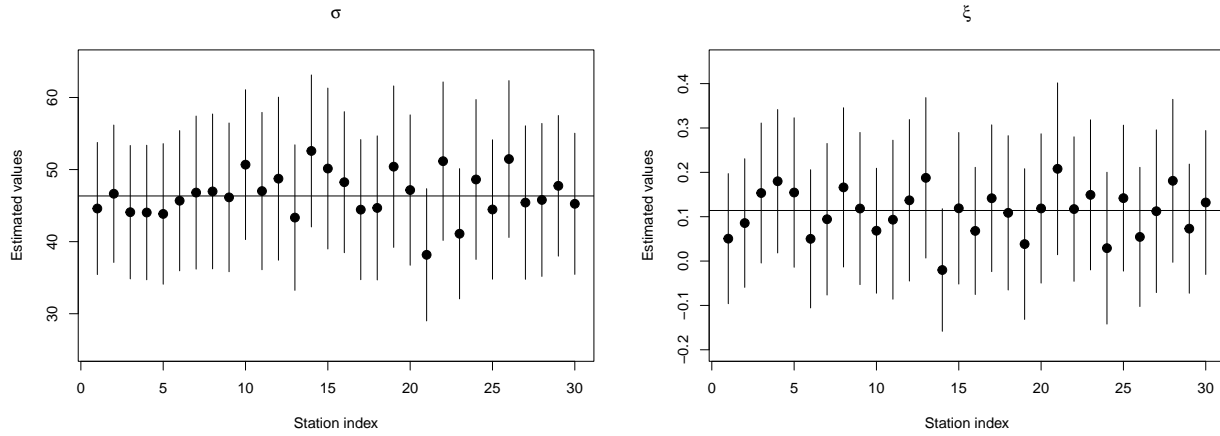


Figure S4: Site-wise estimates (points) and 95% confidence intervals (vertical segments) for σ and ξ . The horizontal lines denote the values estimated on all stations together.

S4. Alternative models

The next Table S2 is the equivalent of Table 1 for the alternative models originating from equation (7) in the main text, which we recall here:

$$X(s, t) = R(s)^\delta W(s, t)^{1-\delta}, \quad \delta \in [0, 1].$$

To prove these results, follow the appendices in the article, carefully inverting the roles of space and time. Results referring to space and space-time can be proven by following [Appendix A](#), while results referring to pairs in time can be proven by following [Appendix B](#).

Model	$R(s)$	$W(s, t)$	$\delta > 0.5$	$\delta = 0.5$	$\delta < 0.5$
5	AI	AD	AI in space AD in time AI in space-time	AI in space AD in time AI in space-time	AD in space AD in time AD in space-time
6	AD	AI	AD in space AD in time AD in space-time	AI in space AI in time AI in space-time	AI in space AI in time AI in space-time
7	AI	AI	AI in space AD in time AI in space-time	AI in space AI in time AI in space-time	AI in space AI in time AI in space-time
8	AD	AD	AD in space AD in time AD in space-time	AD in space AD in time AD in space-time	AD in space AD in time AD in space-time

Table S2: The four possible combinations for $R(s)$ and $W(s, t)$ in (7) and the resulting extremal dependence for pairs $[X(s_1, t_1), X(s_2, t_2)]$ in space, in time and in space-time, for different values of the parameter δ .